

The High Energy X-ray Probe (HEX-P): Constraining Supermassive Black Hole Growth with Population Spin Measurements

J. M. Piotrowska^{1,*}, J. A. García^{2,1}, D. J. Walton³, R. S. Beckmann⁴, D. Stern⁵,
D. R. Ballantyne⁶, D. R. Wilkins⁷, S. Bianchi⁸, P. G. Boorman¹, J. Buchner⁹,
C.-T. Chen^{10,11}, P. Coppi¹², T. Dauser¹³, A. C. Fabian⁴, E. Kammoun^{14,15,8},
K. Madsen², L. Mallick^{16,17,1}, G. Matt⁸, G. Matzeu¹⁸, E. Nardini¹⁵, A. Pizzetti¹⁹,
S. Puccetti²⁰, C. Ricci^{21,22}, F. Tombesi^{23,24,25,26,2}, N. Torres-Albà¹⁹,
K.-W. Wong²⁷, and the HEX-P Collaboration

¹ *Cahill Center for Astronomy and Astrophysics, California Institute of Technology, Pasadena, CA, USA*

² *X-ray Astrophysics Laboratory, NASA Goddard Space Flight Center, Greenbelt, MD, USA*

³ *Centre for Astrophysics Research, University of Hertfordshire, College Lane, Hatfield, UK*

⁴ *Institute of Astronomy, University of Cambridge, Madingley Road, Cambridge, UK*

⁵ *Jet Propulsion Laboratory, California Institute of Technology, Pasadena, CA, USA*

⁶ *Center for Relativistic Astrophysics, School of Physics, Georgia Institute of Technology, Atlanta, GA, USA*

⁷ *Kavli Institute for Particle Astrophysics and Cosmology, Stanford University, Stanford, CA, USA*

⁸ *Dipartimento di Matematica e Fisica, Università Roma Tre, Rome, Italy*

⁹ *Max-Planck-Institut für Extraterrestrische Physik (MPE), Garching bei München, Germany*

¹⁰ *Marshall Space Flight Center, Huntsville, AL, USA*

¹¹ *Science and Technology Institute, Universities Space Research Association, Huntsville, AL, USA*

¹² *Department of Astronomy, Yale University, New Haven, CT, USA*

¹³ *Dr. Karl Remeis-Observatory and Erlangen Centre for Astroparticle Physics, FAU Erlangen-Nürnberg, Bamberg, Germany*

¹⁴ *IRAP, Université de Toulouse, CNRS, UPS, CNES, Toulouse, France*

¹⁵ *INAF – Osservatorio Astrofisico di Arcetri, Firenze, Italy*

¹⁶ *University of Manitoba, Department of Physics & Astronomy, Winnipeg, Manitoba, Canada*

¹⁷ *Canadian Institute for Theoretical Astrophysics, University of Toronto, Toronto, Ontario, Canada*

¹⁸ *Quasar Science Resources SL for ESA, ESAC, Science Operations Department, Madrid, Spain*

¹⁹ *Department of Physics and Astronomy, Clemson University, Kinard Lab of Physics, Clemson, SC, USA*

²⁰ *ASI - Agenzia Spaziale Italiana, Rome, Italy*

²¹ *Instituto de Estudios Astrofísicos, Facultad de Ingeniería y Ciencias, Universidad Diego Portales, Santiago, Chile*

²² *Kavli Institute for Astronomy and Astrophysics, Peking University, Beijing, China*

²³ *Physics Department, Tor Vergata University of Rome, Rome, Italy*

²⁴ *INAF – Astronomical Observatory of Rome, Monte Porzio Catone, Italy*

²⁵ *INFN – Rome Tor Vergata, Rome, Italy*

²⁶ *Department of Astronomy, University of Maryland, College Park, MD, USA*

²⁷ *Department of Physics, SUNY Brockport, Brockport, NY, 14420, USA*

Correspondence*:
Joanna M. Piotrowska
joannapk@caltech.edu

ABSTRACT

Constraining the primary growth channel of supermassive black holes (SMBH) remains one of the most actively debated questions in the context of cosmological structure formation. Owing to the expected connection between SMBH spin parameter evolution and the accretion and merger

history of individual black holes, population spin measurements offer a rare observational window into the SMBH cosmic growth. As of today, the most common method for estimating SMBH spin relies on modeling the relativistically broadened atomic profiles in the reflection spectrum observed in X-rays. In this paper, we study the observational requirements needed to confidently distinguish between the primary SMBH growth channels, based on their distinct spin-mass distributions predicted by the Horizon-AGN cosmological simulation. In doing so, we characterize outstanding limitations associated with the existing measurements and discuss the landscape of future observational campaigns, which can be planned and executed with future X-ray observatories. We focus our attention on the High-Energy X-ray Probe (HEX-P), a concept probe-class mission aimed to serve the high-energy community in the 2030s.

Keywords: supermassive black holes, AGN, black hole growth, black hole spin, future X-ray observatories

1 INTRODUCTION

As of today, the existence of supermassive black holes (SMBHs) residing in the nuclei of galaxies is no longer a subject of scientific dispute. With SMBH presence revealed in the orbital motion of stars in our Galactic centre (e.g. [Ghez et al., 2008](#); [Genzel et al., 2010](#)) and direct imaging of matter just outside the Event Horizon ([Event Horizon Telescope Collaboration et al., 2019, 2022](#)), the focus has now shifted towards understanding the origin and growth of these extreme astrophysical objects with masses above $\gtrsim 10^6 M_{\odot}$. Decades of extragalactic observations have demonstrated a tight connection between the properties of supermassive black holes and their galactic hosts, now interpreted as black hole-galaxy co-evolution across cosmic time (see [Kormendy and Ho, 2013](#), for a review). More specifically, SMBHs have been established as key players in shaping galaxy formation, structure and, most of all, in suppressing galactic star formation through a range of highly energetic processes collectively referred to as Active Galactic Nucleus (AGN) feedback (e.g. [McNamara et al., 2000](#); [Bower et al., 2006](#); [Terrazas et al., 2016](#); [Henriques et al., 2019](#); [Piotrowska et al., 2022](#), among many others).

Regardless of its exact mode of operation, AGN feedback relies on extracting power from the immediate surroundings of supermassive black holes via accretion. The amount of energy released in the process greatly exceeds the threshold required to offset cooling around galaxies or to unbind baryons within them, rendering SMBH a formidable source of power capable of affecting their galactic hosts (see [Fabian, 2012](#); [Werner et al., 2019](#), for in-depth reviews). At high accretion rates ($\dot{M}_{\text{BH}} \gtrsim 0.01 \dot{M}_{\text{Edd}}$, the Eddington accretion rate¹), matter surrounding an SMBH is thought to infall through a geometrically thin, optically thick accretion disk ([Shakura and Sunyaev, 1973](#); [Novikov and Thorne, 1973](#)) in which emitted radiation drives high-velocity *quasar* outflows (e.g. [Murray et al., 1995](#); [King et al., 2008](#); [Faucher-Giguère and Quataert, 2012](#)) coupling to the interstellar medium (ISM) and further accelerating it at galaxy-wide scales (e.g. [Feruglio et al., 2010](#); [Hopkins and Quataert, 2010](#); [Villar-Martín et al., 2011](#); [Maiolino et al., 2012](#); [Cicone et al., 2014](#); [Fiore et al., 2017](#)). At low accretion rates $\lesssim 10^{-6} \dot{M}_{\text{Edd}}$, the inflow forms a geometrically thick, optically thin accretion disk (e.g. [Yuan and Narayan, 2014](#); [Giustini and Proga, 2019](#)) and launches *relativistic jets* which deposit energy within the circumgalactic medium (CGM) at large distances away from the galactic host (e.g. [McNamara et al., 2000](#); [Bîrzan et al., 2004](#); [Hlavacek-Larrondo et al., 2012, 2015](#); [Werner et al., 2019](#)). Across all flavours of AGN feedback processes, the efficiency with which power is extracted from the accretion flow depends on the angular momentum of the SMBH and

¹ Accretion rate associated with Eddington luminosity

spans over an order of magnitude in range (e.g. Thorne, 1974; Penna et al., 2010; Avara et al., 2016; Liska et al., 2019), further broadening the range of impact AGN can have on their host galaxies.

Although abundant observational evidence exists for the impact of supermassive black holes on their surrounding galaxies, relatively little is known about SMBH origin and growth across cosmic time. Understanding how these black holes form and reach their impressive masses is particularly important both in the context of galaxy evolution and recent James Webb Space Telescope (JWST, Gardner et al., 2023; Rigby et al., 2023) observations, which report black holes with masses $M_{\text{BH}} > 10^6 M_{\odot}$ as early as $z = 10.6$ (Harikane et al., 2023; Maiolino et al., 2023a,b). Since cosmic growth via accretion of gas and SMBH-SMBH mergers occurs on timescales beyond direct human observation, one would, ideally, like to characterise supermassive black hole growth histories using alternative observables. An example of such a proxy is black hole angular momentum, \vec{J} , which changes its orientation and magnitude in response to different physical processes increasing M_{BH} . Hence, by *measuring the magnitude of supermassive black hole angular momentum J* , usually expressed in terms of the dimensionless spin parameter ($a^* \equiv Jc/GM_{\text{BH}}^2$, where c is the speed of light and G is the gravitational constant), *one can hope to extract information about the past record of its growth*. In the AGN, spin parameter can be estimated by modelling coronal X-ray radiation reprocessed (or ‘reflected’) by the accretion disk (e.g. Fabian et al., 1989; Laor, 1991). Because the reflected signal depends on the position of the innermost edge of the accretion disk, this relationship can be directly applied to determine a^* in nearby SMBH (see 3.2 for an overview of this approach).

As the black hole increases its mass via accretion of surrounding material, its spin changes owing to angular momentum transfer from the accretion flow. If the accreting material settles into a prograde² disk, inflow of angular momentum aligned with that of the black hole leads to its efficient spin-up (Bardeen, 1970; Moderski and Sikora, 1996; Moderski et al., 1998). In contrast, chaotic accretion of matter with randomly oriented angular momentum decreases the spin magnitude, ultimately driving it towards $a^* \sim 0$ over sufficiently long times (e.g. Berti and Volonteri, 2008; King et al., 2008; Dotti et al., 2013). In the presence of magnetic fields, even in the case of ordered inflow through aligned accretion disks, spin can also be reduced by energy extraction via the Blandford-Znajek process (Blandford and Znajek, 1977). This jet launching mechanism has been shown to drain black hole angular momentum in magnetically arrested disks (MAD) in general-relativistic magneto-hydrodynamical (GRMHD) simulations of SMBH accretion (e.g. Tchekhovskoy et al., 2011; Tchekhovskoy et al., 2012; McKinney et al., 2012; Narayan et al., 2022; Curd and Narayan, 2023; Lowell et al., 2023). Finally, mergers of supermassive black hole binaries leave behind remnants which can be either spun up or down with respect to their progenitors, contingent on individual spin parameters upon coalescence (e.g. Kesden, 2008; Rezzolla et al., 2008; Barausse and Rezzolla, 2009; Tichy and Marronetti, 2008; Healy et al., 2014; Hofmann et al., 2016).

Depending on the relative contribution of these processes across cosmic time, one would expect different growth histories of SMBH to leave an imprint on the measured spin parameter. In the cosmological context, this expectation was first explored in semi-analytic models (SAMs) - taking advantage of their low computational cost, several studies have now used SAMs to make spin population predictions for different SMBH accretion and coalescence scenarios. Berti and Volonteri (2008) demonstrated that prolonged episodes of coherent accretion produce SMBH populations spinning at near-maximal rates, while chaotic infall of matter and mergers force the dimensionless spin parameter towards $a^* \sim 0$. Dotti et al. (2013) generalised the chaotic accretion paradigm and found that SMBHs are not spun down efficiently when the distribution of accreted angular momenta is not isotropic, allowing black holes to maintain stable high spin

² In a prograde disk, the accreting material and the black hole are both rotating in the same direction

values for even modest degrees of anisotropy. By linking the orientation of accreted angular momentum with that of the galactic host, [Sesana et al. \(2014\)](#) further showed that spin parameter critically depends on the dynamics of the host and that SMBH residing in spiral galaxies tend to spin fast, biasing the observable samples towards high a^* values.

Moving beyond the idealised semi-analytic approach, spin parameter modelling in hydrodynamical cosmological simulations only recently became an area of active development ([Dubois et al., 2014c](#); [Fiacconi et al., 2018](#); [Bustamante and Springel, 2019](#); [Talbot et al., 2021, 2022](#)). As of today, there exist three major simulation suites which trace spin parameter in statistical samples of SMBHs. The *NewHorizon cosmological simulation* ([Dubois et al., 2021](#)), on-the-fly spin evolution coupled to AGN feedback prescription in a $(16 \text{ Mpc})^3$ volume; simulated down to $z = 0.25$ at a maximum spatial resolution of 34 pc. The *Bustamante and Springel (2019) simulation suite*, on-the-fly spin evolution implemented in the moving-mesh code AREPO ([Springel, 2010](#)); a cosmological volume of $(\sim 37 \text{ Mpc})^3$ with a spatial resolution of $\sim 1 \text{ kpc}$; evolved to $z = 0$ with the IllustrisTNG AGN feedback model [Weinberger et al. 2017](#). Finally, the *Horizon-AGN cosmological simulation* ([Dubois et al., 2014b](#)), in which spin evolution is computed via post-processing of the completed Horizon-AGN run [Dubois et al. 2014a](#), followed down to $z = 0$ in a $(\sim 147 \text{ Mpc})^3$ volume at maximum spatial resolution of $\sim 1 \text{ kpc}$. All three suites produce realistic populations of SMBH and yield a^* population statistics compatible with those observed in the local Universe. With limited sample sizes and generous uncertainty on individual measurements, currently available observations are not constraining enough to indicate preference for any particular model implementation. In the future, increased measurement precision and improved statistics in the $M_{\text{BH}} - a^*$ plane will be of critical importance for new generations of on-the-fly spin evolution models: with improved calibration targets for subgrid prescriptions, different hydrodynamical cosmological models are likely to further converge over time, allowing us to use a^* constraints as an interpretative tool, as opposed to means of discriminating among modelling approaches.

In this study, we show how future observing programs targeting statistical samples of SMBH spins and masses can be designed to best discriminate between different growth histories of supermassive black holes. We choose to focus on the Horizon-AGN cosmological simulation to take advantage of its excellent SMBH statistics delivered by the substantial simulation volume. Treating the simulation suite as a case study, we estimate sample sizes and measurement precision required to differentiate between accretion- and merger-dominated SMBH growth. We then discuss these requirements in the context of the High-Energy X-ray Probe (*HEX-P*; [[Madsen et al. 2023](#)]) – a probe-class mission concept which offers sensitive broad-band coverage (0.2–80 keV) of the X-ray spectrum with exceptional spectral, timing and angular capabilities, featuring two high-energy telescopes (HET) that focus hard X-rays, and soft X-ray coverage with a single low-energy telescope (LET). Taking into account the *HEX-P* instrument design, we explicitly demonstrate the potential for this probe class mission to deliver SMBH spin parameter measurements necessary for constraining supermassive black hole growth in the observable Universe.

In Section 2 we discuss the challenges associated with spin modelling in cosmological hydrodynamical simulations and briefly describe the Horizon-AGN suite. In Section 3 we provide an overview of reflection spectroscopy as a tool for measuring a^* , followed by a discussion on current constraints and their comparison with the Horizon-AGN cosmological model in Section 4. In Section 5 we advocate for a systematic study of the $M_{\text{BH}} - a^*$ plane with future observing programs and in Section 6 we describe a sample of AGN selected from the BAT AGN Spectroscopic Survey appropriate for such study. In Section 7 we determine minimum sample requirements for differentiating between accretion- and merger-dominated SMBH growth, followed by *HEX-P* spin parameter recovery simulation in Section 8.3. In Section 9 we

demonstrate the potential for *HEX-P* to characterise SMBH growth histories through population spin measurements and present our final remarks in Section 10.

2 SMBH SPIN IN COSMOLOGICAL HYDRODYNAMICAL SIMULATIONS

Tracing the change in supermassive black hole (SMBH) spin in the context of large-scale evolution of the Universe is an extraordinarily complex problem spanning a broad range of spatial and temporal scales. Transfer of angular momentum via accretion in disks occurs on size scales between ~ 1 and a few 10^2 gravitational radii $R_G = GM_{\text{BH}}/c^2$ (e.g. Jiang et al., 2017; Cackett et al., 2018; Fausnaugh et al., 2016; Edelson et al., 2019; Guo et al., 2022; Homayouni et al., 2022), which then couples to gas inflows from host galaxy scales of several hundred pc (e.g. García-Burillo et al., 2005; Hopkins and Quataert, 2010; Alexander and Hickox, 2012; Wong et al., 2011, 2014; Russell et al., 2015, 2018), ultimately fuelled by gas accretion from within the cosmic web at the intergalactic scales of hundreds of kpc (e.g. Sancisi et al., 2008; Putman et al., 2012; Tumlinson et al., 2017). At the same time, gas flows at all scales are affected by the non-trivial interplay of feedback processes from both stars (e.g. Katz et al., 1996; Cole et al., 2000; Kereš et al., 2005; Hopkins et al., 2014) and active galactic nuclei, AGN (e.g. Bower et al., 2006; Croton et al., 2006; Fabian, 2012; Kormendy and Ho, 2013), disk instabilities (e.g. Schwarz 1981; Athanassoula et al. 1983; Kuijken and Merrifield 1995; Debattista et al. 2006) and galaxy-galaxy interactions (e.g. Toomre and Toomre 1972; Sanders et al. 1988, Barnes and Hernquist 1992; Di Matteo et al. 2005; Springel et al. 2005; Hopkins et al. 2006) all of which, ideally, need to be taken into account in a comprehensive modelling of SMBH spin evolution. The dynamic range in size scales alone renders it computationally unfeasible to directly follow SMBH evolution even with current state-of-the-art hardware and numerical methods (see Vogelsberger et al., 2020; Crain and van de Voort, 2023, for reviews of the current state of the field). Hence, to overcome these limitations, cosmological simulations replace missing baryonic physics with *subgrid*³ prescriptions - semi-analytic models relying on astrophysical scaling relations to predict large scale hydrodynamic effects of unresolved AGN accretion, spin evolution and feedback.

There currently exist three cosmological hydrodynamical simulations which either model spin on-the-fly (Bustamante and Springel, 2019; Dubois et al., 2021) or calculate its evolution in post-processing (Dubois et al., 2014b) (see Section 1). Although these three studies differ significantly in their subgrid prescriptions, in addition to spanning different cosmological volumes and final simulation redshift, they all deliver SMBH spin populations broadly consistent with the currently available observational constraints. As spin modelling in full cosmological context is still in its infancy, the agreement between both models themselves and with the observable Universe is likely to improve, once better constraints are available for subgrid parameter tuning. Thus, the study presented in this article does not focus on differentiating among currently available models, but rather on demonstrating the capability of *HEX-P* to identify different SMBH growth channels within a single realisation of a sophisticated full-physics model of the Universe.

2.1 Horizon-AGN cosmological model

In our study we make use of the Horizon-AGN cosmological simulation (Dubois et al., 2014a), post-processed to trace SMBH spin evolution in response to local hydrodynamics of gas, accretion and SMBH mergers (Dubois et al., 2014b). Our choice of the simulation suite is motivated by its substantial volume of ($\sim 100\text{cMpc}$)³, generous statistics and great success in reproducing realistic SMBH and galaxy samples across cosmic time (Dubois et al., 2016; Volonteri et al., 2016; Beckmann et al., 2017; Kaviraj et al., 2017).

³ Capturing physics at scales smaller than those allowed by numerical resolution via semi-analytic prescriptions coupled to quantities directly resolved in the simulation. See Vogelsberger et al. (2020) and Crain and van de Voort (2023) for comprehensive reviews of the methodology.

Most importantly, however, accretion-dominated and accretion & merger growth histories of supermassive black holes in Horizon-AGN have been shown to result in distinct spin parameter distributions (Beckmann et al., 2023), hence the suite offers a promising opportunity for studying the SMBH growth signal with *HEX-P* reflection spectroscopy. The full Horizon-AGN suite, together with its spin parameter evolution model are described in detail in Dubois et al. (2014a) and Dubois et al. (2014b) and here we only provide a brief overview of SMBH treatment in the simulation.

Horizon-AGN is a suite of cosmological, hydrodynamical simulations performed with the RAMSES code (Teyssier, 2002) for Λ CDM cosmology with cosmological parameter values estimated in WMAP-7 observations ($H_0 = 70.4 \text{ km s}^{-1} \text{ Mpc}^{-1}$, $\Omega_m = 0.272$, $\Omega_b = 0.045$, $\Omega_\Lambda = 0.728$ and $\sigma_8 = 0.81$; Komatsu et al. 2011). The hydrodynamics computed on an adaptively refined Cartesian grid is coupled to subgrid prescriptions for baryonic interactions, including gas cooling, star formation, black hole accretion and feedback processes described in detail in Dubois et al. (2014a). The simulation only includes black holes of the supermassive kind, seeding them in $z > 1.5$ gas cells once these exceed a star formation threshold of $n_0 = 0.1 \text{ H cm}^{-1}$ in density. Once seeded, the SMBH then accrete via a boosted Bondi-Hoyle-Lyttleton prescription ($\dot{M}_{\text{BH}} = 4\pi\alpha G^2 M_{\text{BH}}^2 \bar{\rho} / (\bar{c}_s^2 + \bar{u}^2)^{3/2}$, where \bar{u} , $\bar{\rho}$ and \bar{c}_s are gas velocity, density and speed of sound averaged in the SMBH vicinity, and G is the gravitational constant; Hoyle and Lyttleton 1939; Bondi and Hoyle 1944; Bondi 1952) capped at the Eddington rate. A fraction $\epsilon_r = 0.1$ of the accreted rest-mass energy is then released as AGN feedback with $\dot{E}_{\text{AGN}} = \epsilon_r \dot{M}_{\text{BH}} c^2$, where c is the speed of light, and the fraction of power coupled to gas is controlled by the accretion rate-dependent feedback mode. For Eddington ratios $f_{\text{Edd}} \equiv \dot{M}_{\text{BH}} / \dot{M}_{\text{Edd}} > 0.01$, the AGN is in the ‘quasar’ mode and isotropically injects $0.15 \dot{E}_{\text{BH}}$ as thermal energy around the SMBH particle. For $f_{\text{Edd}} < 0.01$ the AGN switches to ‘radio’ mode feedback, releasing all \dot{E}_{BH} in biconical outflows. In a post-processing procedure introduced in Dubois et al. (2014b), SMBH are assumed to begin with a spin of $a^* = 0$, which subsequently evolves in response to accretion of gas from the hydrodynamical grid and SMBH-SMBH mergers across cosmic time. The spin evolution model combines semi-analytic considerations and calibrations extracted from GRMHD simulations to model the two phenomena, including spin evolution in misaligned disks via the Bardeen-Peterson effect. The prescription, however, does not model SMBH spin-down due to jets via the Blandford-Znajek mechanism.

3 OBSERVATIONS OF BLACK HOLES

Astrophysical black holes are unique objects of great interest as they represent the ultimate test of general relativity as a theory for gravity. Despite their exotic phenomenology, black holes are also objects of outstanding simplicity; owing to the no-hair theorem (Israel, 1967, 1968; Carter, 1971), they are fully described by only three physical quantities: mass, angular momentum (or spin), and electric charge. Furthermore, charge is quickly neutralized in any realistic astrophysical environment (Michel, 1972; Wald, 1984; Novikov and Frolov, 1989; Treves and Turolla, 1999; Bambi, 2017), leaving just mass and spin as the fundamental parameters to be constrained by observations.

3.1 Mass

Of the two properties describing a black hole, mass is likely the most straightforward to measure (both for stellar and supermassive black holes; SMBHs). Indeed, a range of techniques has now been developed for SMBH mass estimation, appropriate for both local and distant sources. For a relatively nearby system (such as the SMBH in the center of our Galaxy), it is possible to resolve the motion of individual stars and model the underlying gravitational potential to estimate its associated black hole mass (e.g. Ghez et al.

1998; Ghez et al. 2008; Genzel et al. 2010; Gravity Collaboration et al. 2018). Owing to extremely high resolution requirements, such studies can only be undertaken within the Milky Way, while extragalactic M_{BH} measurements are instead forced to rely on stellar, gas and maser kinematics (e.g. Kormendy et al. 1998; Magorrian et al. 1998; Gebhardt et al. 2000).

One of the most robust methods for measuring M_{BH} for active SMBHs in other galaxies involves reverberation mapping of broad emission lines (Blandford and McKee, 1982; Peterson, 1993). In this approach, velocity dispersion of gas in the broad line region (BLR) is combined with a measurement of the time delay between variations in the continuum and the line emission to infer the dynamics of the accretion disks (see e.g. Peterson et al., 2004, for a description of the methodology). The mass estimate relies on the proportionality⁴ $M_{\text{BH}} \propto R_{\text{BLR}}(\Delta V)^2$ between SMBH mass, the line-of-sight velocity of BLR gas (ΔV , encoded in emission line profiles) and the distance between the black hole and the BLR (R_{BLR} , inferred from the time lag measurement). Since observations of this kind require long exposure times at prime facilities, the current sample of M_{BH} measured via reverberation contains only ~ 100 objects in total (e.g. Woo et al. 2015).

Because of the limited number of direct SMBH mass measurements, large statistical studies commonly rely on empirical calibrations to estimate M_{BH} from the measured properties of their galactic hosts. Among these, the relationship between stellar velocity dispersion in the galactic bulge and SMBH mass measured via reverberation mapping, the $M_{\text{BH}} - \sigma_*$ relation, boasts the least scatter, yielding a systematic uncertainty of $\sim 0.3 - 0.5$ dex in $\log(M_{\text{BH}})$ (Ferrarese and Merritt, 2000; Hopkins et al., 2011; McConnell and Ma, 2013; Saglia et al., 2016). Although subject to significant scatter at present, these calibrations will improve with the arrival of future large multi-epoch observation programs like the Black Hole Mapper (Kollmeier et al., 2019). The planned ~ 1000 optical reverberation mapping M_{BH} estimates will significantly increase the robustness and precision of the $M_{\text{BH}} - \sigma_*$ estimation. Other techniques have also been recently proposed to measure M_{BH} using X-ray variability, such as X-ray reverberation (Alston et al., 2020) and X-ray spectral-timing (Ponti et al., 2012; Ingram et al., 2022), both of which can be model dependent and carry systematic uncertainties that still need to be understood.

3.2 Spin

The estimation of black hole spin, on the other hand, is a somewhat more difficult task, as it mainly impacts the environment very close to the black hole. For example, the black hole's angular momentum determines the radius of the innermost stable circular orbit, ISCO (R_{ISCO} , which varies from $9 R_{\text{G}}$ for a maximal retrograde spin to $\sim 1.2 R_{\text{G}}$ for a maximal prograde spin of $a^* = 0.998$, where $R_{\text{G}} = GM_{\text{BH}}/c^2$ is the gravitational radius; Bardeen et al. 1972; Thorne 1974). In principle, the spin of a black hole can be constrained through a variety of methods, most of which involve determining R_{ISCO} , but for AGN the most reliable method currently available comes via the characterization of the relativistic reflection from the innermost accretion disk (sometimes referred to as the iron-line method; see Reynolds 2021 for a recent review).

For moderately high accretion rates most of the infalling material is expected to flow through a thin, optically-thick accretion disk (Shakura and Sunyaev 1973). Some of the thermal emission from the disk, which peaks in the UV for most AGN, is Compton up-scattered into a much higher energy continuum by a 'corona' of hot electrons ($kT_e \sim 100$ keV; Fabian et al. 2015; Baloković et al. 2020), which is the primary

⁴ The proportionality constant, known as the virial factor, is challenging to determine for individual objects owing to the unknown geometry of the BLR gas (e.g. Brewer et al., 2011; Pancoast et al., 2014)

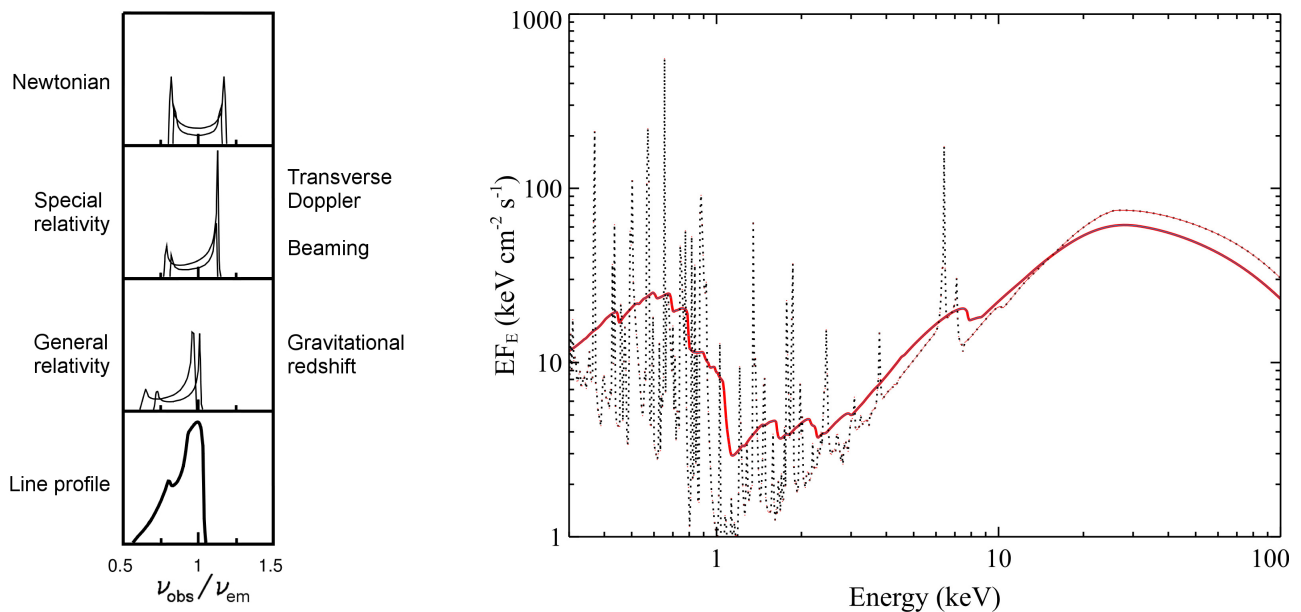


Figure 1. *Left panel:* The broadening experienced by a narrow emission line from an accretion disk around a black hole (from Fabian et al. 2000). The top three panels show the effects of Newtonian gravity, special relativity and general relativity, respectively, on the line profiles for two example radii within the disk, while the bottom panel shows the broadened and skewed ‘diskline’ profile expected when these combined effects are integrated over the full radial profile of the disk. *Right panel:* An example of these relativistic effects applied to a typical reflection spectrum from moderately ionised material (as may be expected for the accretion disk in an AGN). Here we use the XILLVER reflection model for the rest-frame reflection spectrum (dotted line; García and Kallman 2010) and apply the relativistic blurring with the RELCONV model (solid line; Dauser et al. 2010).

source of X-ray emission in AGN⁵. This X-ray emission re-irradiates the surface of the disk, producing a further ‘reflected’ emission component that contains a diverse range of atomic spectral features both in emission and absorption. Among these, the inner-shell transitions from iron ions - predominantly the $K\alpha$ emission line at 6.4–6.97 keV (depending on the ionisation state) - together with a strong absorption K-edge around 7 – 8 keV, are typically the most prominent. Additionally, reflection spectra exhibit a characteristic high-energy continuum, peaking at ~ 30 keV, often referred to as the ‘Compton hump’ (George and Fabian 1991; Ross and Fabian 2005; García and Kallman 2010). Although the emission lines are narrow in the frame of the disk, by the time the material in the disk approaches the ISCO it is orbiting at relativistic speeds, and the gravitational redshift is also very strong. The combination of these effects serves to broaden and skew the emission lines from our perspective as a distant, external observer, resulting in a characteristic ‘diskline’ emission profile (Fabian et al. 1989; Laor 1991; Brenneman and Reynolds 2006; Dauser et al. 2010; see Figure 1). Provided that the disk extends all the way into the innermost stable circular orbit, also expected at moderately high accretion rates, then characterising the relativistic blurring gives a measurement of R_{ISCO} , and thus of a^* . These distortions are most often discussed in the context of the iron emission line specifically, as it is typically the strongest spectroscopically isolated emission line in the reflection spectrum. While the iron emission provides the cleanest view of the broadened line profile, in reality, these relativistic effects impact the whole reflection spectrum (see also Figure 1).

⁵ The precise nature of the corona is still poorly understood, but is also an area of AGN physics that *HEX-P* will make significant contributions to ([Kammoun et al. 2023])

This approach to measuring spin is particularly powerful as it can be applied to black holes of all masses, not just the SMBHs powering AGN (e.g. Walton et al. 2012). Indeed, relativistically broadened Fe K lines have been observed in the spectra of a large fraction of AGN with high signal-to-noise (S/N) X-ray spectra (e.g. Tanaka et al. 1995; Miniutti et al. 2007; Fabian et al. 2009; de La Calle Pérez et al. 2010; Brenneman et al. 2011; Nardini et al. 2011; Gallo et al. 2011; Parker et al. 2014; Ricci et al. 2014; Wilkins et al. 2015; Jiang et al. 2018; Walton et al. 2019) as well as most well-studied BH X-ray binaries (e.g. Miniutti et al. 2004; Miller et al. 2009; Reis et al. 2009; Duro et al. 2011; King et al. 2014; García et al. 2015; Walton et al. 2017; Xu et al. 2018; Kara et al. 2019; Tao et al. 2019; Jiang et al. 2022; Draghis et al. 2023; see also [Connors et al. 2023] for more discussion on BH X-ray binaries with *HEX-P*). Broadband X-ray spectroscopy is particularly critical for properly characterising the reflected emission: its key features span the entire observable X-ray band (a diverse set of emission lines from lighter elements at energies $\lesssim 2$ keV, the iron emission line at $\sim 6\text{--}7$ keV and the Compton hump at ~ 30 keV) and their proper modelling requires an accurate characterisation of the continuum across the entire broadband range. The *NuSTAR* era has therefore marked a period of excellent recent progress in this field, finally providing high S/N spectroscopy up to ~ 80 keV for AGN. *NuSTAR* observations have unambiguously revealed the high-energy reflected continuum associated with the broad iron emission, and have been particularly powerful when paired with simultaneous lower-energy coverage from e.g. *XMM-Newton*, confirming our ability to measure spin via reflection spectroscopy (e.g. Risaliti et al. 2013; Walton et al. 2014; Marinucci et al. 2014; Buisson et al. 2018; García et al. 2019; Chamani et al. 2020; Wilkins et al. 2022). As we further show in Section 4, however, these currently available samples of measurements with X-ray reflection spectroscopy are still not sufficient for characterising SMBH growth histories in the observable Universe.

4 CURRENT CONSTRAINTS: THE SPIN–MASS PLANE

The most recent systematic compilations of SMBH spins and masses from the literature are presented in Reynolds (2021) and Bambi et al. (2021), although there have been a few more measurements made since the publication of these reviews (Walton et al. 2021; Mallick et al. 2022; Sisk-Reynés et al. 2022), resulting in a current sample size of 46 SMBHs with at least initial spin constraints. All but three of these sources are from the local Universe ($z \leq 0.3$, and even then most have $z \leq 0.1$); the two highest redshift constraints to date come from strongly-lensed quasars ($z = 0.66$ and $z = 1.7$; Reis et al. 2014; Reynolds et al. 2014).

Fig. 2 shows the current constraints in the spin-mass plane for SMBH with masses above $10^6 M_\odot$. Grey filled diamonds indicate measurements with 1σ error bars⁶, while open diamonds mark lower limits on a^* . Many of the measurements show evidence for rapidly rotating black holes, particularly for masses in the range $M_{\text{BH}} \sim 10^6 - 10^7 M_\odot$. There are hints in the current data of trends towards lower spins, or at least an increase in the spread of spin measurements, at higher masses particularly for $M_{\text{BH}} > 10^8 M_\odot$. In order to better capture these trends we further calculate mean spin parameter values in three bins of SMBH mass between 10^6 and $10^{10} M_\odot$ ⁷, marked with open black squares. In the mean calculation we treat all available constraints as uncensored measurements and hence arrive at lower limit estimates in each bin, which indicate a tentative decrease in a^* with increasing M_{BH} . We note, however, that there are still only a few measurements in the high-mass regime, and the uncertainties on those are also still quite poor. Furthermore, although a few sample-based efforts to constrain SMBH spin via systematic relativistic reflection analyses exist (e.g. Walton et al., 2013; Mallick et al., 2022), the majority of these measurements

⁶ Measurements reported in the literature commonly quote 90% confidence intervals for spin parameter measurements. In order to translate these values to 1σ estimates, we divide the confidence interval by a factor of 1.64, necessarily assuming that the current constraints follow split normal distributions

⁷ Our choice of binning scheme is discussed in Section 7.1

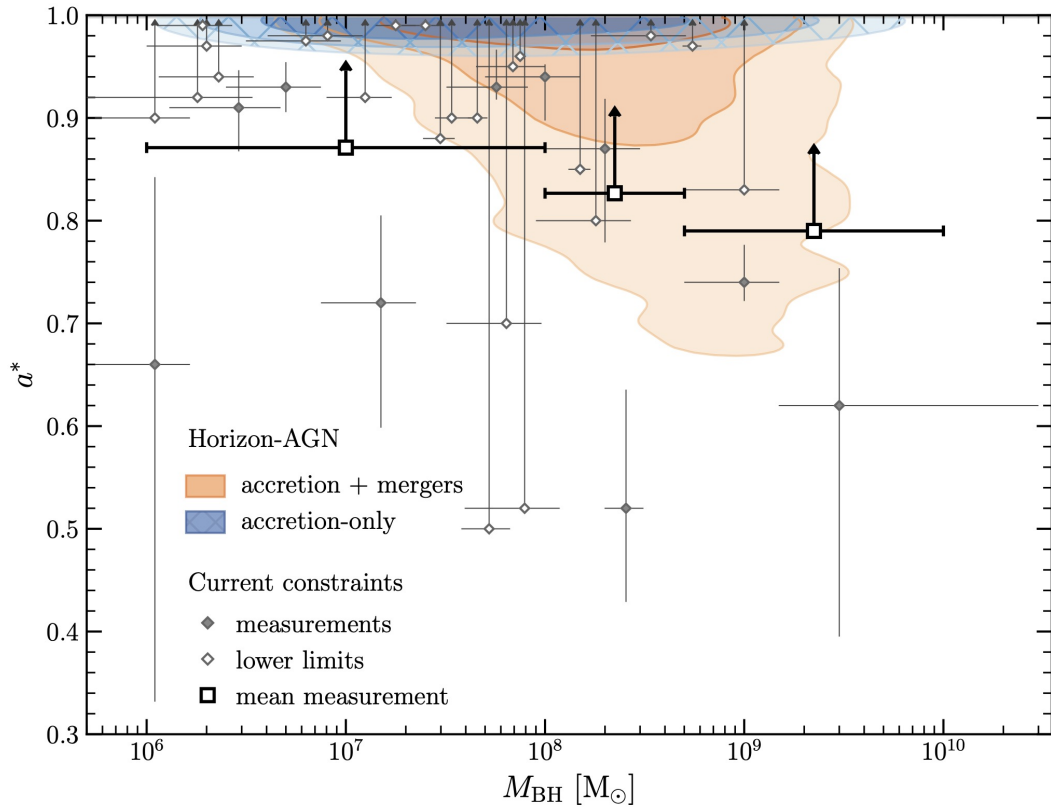


Figure 2. Current observational constraints in the $M_{\text{BH}} - a^*$ plane (open and filled grey diamonds), compared against the locus occupied by the HorizonAGN cosmological simulation (logarithmically spaced contours) for black holes with $M_{\text{BH}} \geq 10^6 M_{\odot}$ (the range covered by Horizon-AGN). Error bars associated with filled diamonds indicate 1σ uncertainty on a^* measurement. Blue, hatched: SMBHs which acquired less than 10% of their mass in mergers (i.e. accretion-only growth), orange: SMBH with $> 10\%$ mass grown in mergers (i.e. accretion + mergers growth). Both contours account for the radiative efficiency - spin bias in flux-limited AGN samples. Existing constraints indicate a decreasing trend in a^* with M_{BH} , as shown by lower limits on mean a^* values in M_{BH} bins (black open squares), however are not able to differentiate between SMBH growth scenarios (orange vs. blue contours).

come from independent analyses of individual sources. As such, they are quite heterogeneous with regards to the exact reflection and relativistic blurring models used, the precise assumptions adopted in the use of these models, and the energy range over which the analysis has been performed; moreover, *NuSTAR* has only contributed to \sim half of these measurements, so not all of them are based on high S/N broadband X-ray spectroscopy.

Perhaps one of the most important caveats associated with current spin measurement constraints is the target selection. In a collection of independent observations, as opposed to a survey campaign, it is challenging to properly control for the sample selection function and, by extension, observational biases present in the combined dataset. Among these, a potential bias towards high a^* values resulting from the expected spin-dependence of the radiative efficiency ($\eta(a^*)$) in a relativistic thin-disk solution (Novikov and Thorne, 1973) is frequently discussed in the literature as at least part of the reason for the observed prevalence of near-maximal spin values (e.g. Brenneman et al., 2011; Reynolds et al., 2012). Under the simplifying assumption of a uniform distribution of AGN in the local Universe, the probability of observing a given spin value a^* scales with $\eta(a^*)$ to power $3/2$ for sources with equal accretion rates in flux-limited

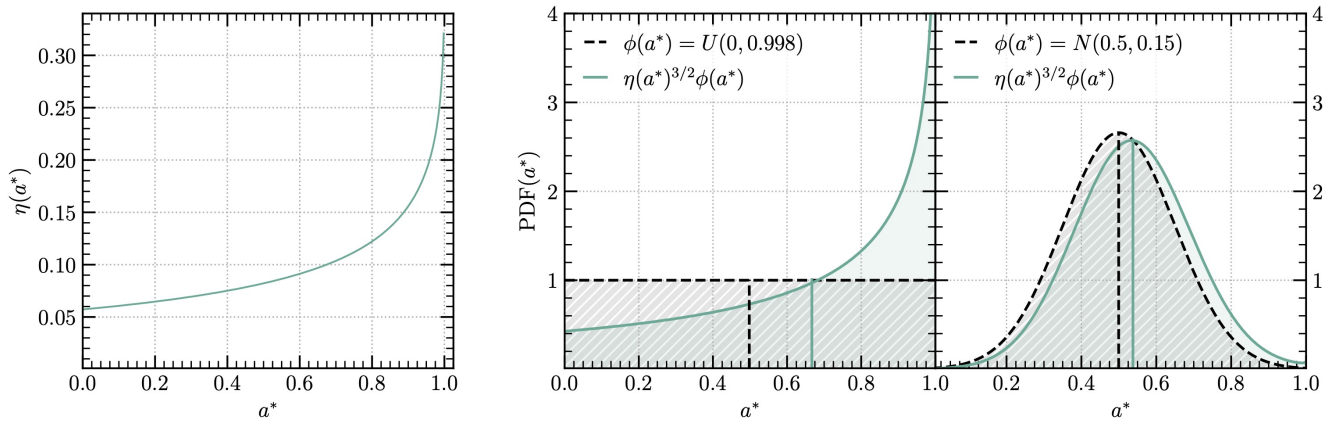


Figure 3. *Left panel:* efficiency $\eta(a)$ as a function of spin parameter a for a thin disk solution (Novikov and Thorne, 1973). *Right panels:* the effect of spin-dependence of η on the measurement spin population statistics, illustrated with changes to the probability distribution function (PDF, shaded regions) and its associated mean spin parameter value (vertical lines). Grey hatched regions in the middle and rightmost panels correspond to ‘raw’ PDFs for a uniform distribution $a^* \sim U(0, 0.998)$ and a normal distribution centered on $a^* = 0.5$ with $\sigma = 0.15$, respectively, while their coloured counterparts to PDFs corrected for the $\eta - a^*$ bias. The shift between dashed and solid vertical lines indicates the change in associated mean a^* value between raw (dashed) and η -bias corrected distributions (solid). The magnitude of bias critically depends on the true underlying spin parameter PDF.

surveys (see Appendix for further details). The superlinear scaling combined with steep increase of $\eta(a^*)$ at $a^* > 0.8$ can have profound implications for inferred spin population statistics in observations.

Fig. 3 shows the change in radiative efficiency with spin in geometrically thin relativistic disks (left panel) together with the potential impact the $\eta - a^*$ bias can have on the observed spin parameter distributions (two panels on the right). Using a uniform distribution of $a^* \sim U(0, 0.998)$ and a normal distribution $a^* \sim N(0.5, 0.15)$ as examples, the two panels on the right demonstrate how a probability distribution function (PDF) of the expected measurements is distorted towards high spin values, shifting the expected mean observed spin values towards $a^* \approx 0.67$ and $a^* \approx 0.54$ for the two respective input distributions. As demonstrated in the figure, the impact of the $\eta - a^*$ bias is critically dependent on the underlying true spin parameter distribution. Therefore, the strength of this effect will differ from our test cases for realistic samples of AGN observations.

4.1 Connecting to SMBH growth histories in Horizon-AGN

As discussed in Sec 2, different modes of SMBH growth leave distinct imprints on their angular momenta. Hence, once integrated over the lifetime of individual black holes, one would expect different SMBH growth histories, e.g. accretion- vs. merger-dominated scenarios, to yield distinguishable predictions for the measurement of their spin parameter a^* . Indeed, Beckmann et al. 2023 (hereafter B23) study the existence of such signatures in the $z = 0.0556$ snapshot of the Horizon-AGN cosmological simulation, finding that black holes grown exclusively via accretion (nearly merger-free) have a spin distribution that is distinct from the rest of the black hole population at $> 5\sigma$ significance. As shown in Fig. 3 in B23, SMBHs which acquired $< 10\%$ of their mass in mergers have a significantly narrower distribution of spin parameter values than the remainder of the black hole population, concentrated at spin values close to $a^* = 0.998$. The striking contrast between a^* populations reported by the authors presents a promising prospect for

extending the study into two dimensions - distinguishing SMBH growth histories with measurements in the $M_{\text{BH}} - a^*$ plane.

To extract predictions for the observable signatures of different SMBH growth histories in the spin-mass plane from Horizon-AGN, we first identify the loci occupied by each history in the $M_{\text{BH}} - a^*$ parameter space. From here onwards we focus on the $z = 0.0556$ snapshot of the simulation studied in B23, which is well suited for our intended target sample of local AGN (see Section 6.1). Inspired by B23, we use a threshold on $f_{\text{BH, merge}}$, the fraction of mass acquired in mergers, to identify the *accretion-only* and *accretion+mergers* growth channels. We adopt $f_{\text{BH, merge}} < 0.1$ for accretion-only and $f_{\text{BH, merge}} > 0.1$ for accretion+mergers, which yield populations of 2137 and 4714 black holes respectively. Since the accretion-only population in the simulation is limited to $M_{\text{BH}} < 10^{8.5} M_{\odot}$, to showcase its spin predictions across the entire mass range in Fig. 2, we extend the dataset over the missing M_{BH} range with random draws from the accretion-only a^* probability density function (PDF). More specifically, we calculate the accretion-only PDF for $M_{\text{BH}} > 10^8 M_{\odot}$ and take random draws from it to generate $M_{\text{BH}} - a^*$ value pairs with M_{BH} distribution matching that of the accretion+mergers population beyond $10^8 M_{\odot}$. In this way we mimic the effect of switching off spin evolution due to merger events studied for the $z = 0$ snapshot in Dubois et al. (2014b) (see Fig. 7 in the publication), arriving at an expected a^* measurement across the whole range in M_{BH} for the accretion-only growth channel. We note that although the Eddington-limited subgrid model for SMBH in Horizon-AGN does not produce merger-free populations at very high M_{BH} , one could still expect highly spinning black holes at the high-mass end from models which include super-Eddington accretion rates in cosmological hydrodynamical simulations (e.g. Massonneau et al., 2023)⁸.

Fig. 2 compares loci in the $M_{\text{BH}} - a^*$ plane occupied by black holes with accretion-only (blue hatched contours) and accretion+mergers (orange filled contours) growth histories in Horizon-AGN. Current observational constraints for $M_{\text{BH}} > 10^6 M_{\odot}$ are shown as individual grey points, with open diamonds corresponding to lower limits and filled diamonds representing measurements and their corresponding 1σ uncertainties. To ensure a meaningful comparison between observations and the cosmological simulation, both of the 2D spin distributions extracted from Horizon-AGN are corrected for the $\eta(a^*) - a^*$ bias and hence are vertically shifted upwards with respect to the raw output of the simulation. Fig. 2 clearly demonstrates that the *two SMBH growth scenarios yield different signatures in the spin-mass parameter space*. At $M_{\text{BH}} \gtrsim 10^8 M_{\odot}$ the two growth histories begin separating, with mergers pushing the expected spin parameter values down towards values as low as $a^* \sim 0.6$ with increasing M_{BH} , while the accretion-only scenario remains concentrated at near-maximal spin values. For black hole masses $< 10^8 M_{\odot}$ both accretion-only and accretion+mergers populations are concentrated around near-maximal a^* values. This degree of overlap is further exacerbated by the spin-dependent radiative efficiency correction, which shifts the orange contours upwards, bringing the two populations towards near-identical loci. Overall, in the context of the Horizon-AGN cosmological simulation, Fig. 2 presents a promising opportunity for differentiating between SMBH growth channels in X-ray observations of AGN, even in the presence of the expected $\eta(a^*) - a^*$ bias.

5 THE NEED FOR A SYSTEMATIC STUDY OF THE SPIN-MASS PLANE

Another critical conclusion drawn from Fig. 2 is the necessity of obtaining high-precision spin measurements for large statistical samples of local AGN. Although the current observational constraints

⁸ We also note that efficient SMBH merging is, in part, a consequence of the limitations associated with modelling black hole mergers in cosmological simulations, which do not explicitly follow the SMBH orbital angular momentum loss via dynamical friction

are broadly consistent with the accretion+mergers growth channel and show a hint of decrease in a^* with M_{BH} above $10^8 M_{\odot}$, the limited number of measurements at these masses and the relatively poor precision of these measurements mean the current data are not sufficient for a statistical assessment of these trends. More importantly for our discussion, the current sample of 10 measurements and 23 upper limits presented in the figure is not capable of differentiating between the two signatures of SMBH growth histories predicted by Horizon-AGN.

The current state-of-the-art spin measurements also offer a rather limited opportunity for the validation and improvement of the SMBH spin evolution models used in cosmological simulations of SMBH growth. When compared against other hydrodynamical simulations which cover a similar range in M_{BH} (Bustamante and Springel, 2019), Horizon-AGN produces spin population statistics with only subtle differences in their $M_{\text{BH}} - a^*$ loci. In general this is encouraging, as it suggests that the qualitative trends implied by these simulations (i.e. Figure 2) are robust. The discrepancies that do exist between them, however, are a combined result of differences in subgrid prescriptions for SMBH seeding, accretion and feedback, and hence carry important information about the validity of a given numerical approach. With the measurement precision and sample size offered by the current constraints, one cannot determine which model implementation (if any) is a closer approximation of the observable Universe. Consequently, the current constraints allow enough room to validate a range of models, while, at the same time, are not strong enough to serve as observational calibrators for future generations of subgrid cosmological SMBH models.

In summary, Fig. 2 demonstrates that *a systematic study of the spin-mass plane is necessary for differentiating between different growth histories of SMBHs in the local Universe*. A comprehensive characterisation of M_{BH} and a^* properties of local AGN will also play a critical role in calibrating subgrid models of cosmological structure formation by delivering improved constraints on physical properties of SMBH. To establish measurement requirements for these survey observations we take the two SMBH growth histories in Horizon-AGN as a case study, and investigate the precision and sample sizes that would be required to differentiate between these two possibilities in realistic samples of observable sources.

6 THE BASS SAMPLE

In order to assess the number of known AGN for which spin constraints may be possible, either now or in the moderately near future, we turn to the BAT AGN Spectroscopic Survey (BASS; Koss et al. 2017). This is a major multi-wavelength effort to characterise AGN detected in the very high energy X-ray survey conducted by the Burst Alert Telescope (BAT, 14–195 keV; Barthelmy et al. 2005) onboard the *Neil Gehrels Swift Observatory* (hereafter *Swift*; Gehrels et al. 2004). The latest 105-month release of the BAT source catalogue (Oh et al. 2018) contains 1632 sources in total, of which 1105 have been identified as some kind of AGN. BASS provides black hole mass estimates (drawn from a variety of methods including $H\beta$ line widths, stellar velocity dispersions and literature searches⁹) and Eddington ratios for the majority of these (e.g. Koss et al. 2022), as well as initial constraints on their broadband spectral properties by combining the BAT data with the best soft X-ray coverage available (e.g. from *XMM-Newton*; Ricci et al. 2017).

6.1 Sources with spin measurement potential

Not all AGN are well suited to making spin measurements. In particular, the very hard X-ray selection of the BAT survey means it is sensitive to even heavily obscured AGN (including ‘Compton thick’ sources with $N_{\text{H}} > 1.5 \times 10^{24} \text{ cm}^{-2}$; e.g. Arévalo et al. 2014; Annuar et al. 2015), and determining the contribution from

⁹ The method used to estimate the mass for each source is also provided in the BASS catalogue.

relativistic reflection becomes increasingly challenging as the source becomes more obscured. Furthermore, there is a general expectation that at low accretion rates the optically-thick accretion disk becomes truncated at radii larger than the ISCO (Narayan and Yi 1994; Esin et al. 1997; Tomsick et al. 2009), such that the inner radius of the disk no longer provides direct information about the spin. As such, in order to compile a sample of AGN for which spin measurements should be possible, we apply several selection criteria to the BASS sample. First, we select sources with fairly low levels of obscuration, requiring a neutral column density of $N_{\text{H}} \leq 10^{22} \text{ cm}^{-2}$. Second, we select sources with Eddington ratios of $\lambda = L_{\text{bol}}/L_{\text{Edd}} \geq 0.01$, so that we may have confidence that the accretion disk should extend to the ISCO (note also that this selection naturally means a black hole mass estimate is available, otherwise it would not have been possible to estimate λ). We further place an upper limit of $\lambda < 0.7$ to select sources for which thin disk approximation is appropriate (e.g. Steiner et al., 2010). We also require that the sources exhibit sufficiently strong reflection features in order for spin measurements to be feasible. We therefore then select sources for which the initial X-ray spectroscopy conducted by Ricci et al. (2017) indicates a reflection fraction consistent with $R \geq 1$ (note that Ricci et al. 2017 use the definition of the reflection fraction from Magdziarz and Zdziarski 1995). For the same reason, we also exclude blazars from our sample. Finally, after having made these cuts to the BASS data, we also exclude a small number of remaining sources for which the initial X-ray spectroscopy implies an unreasonably hard photon index ($\Gamma \leq 1.5$), taking this as an indication that either the source is actually obscured but that the absorption is sufficiently complex that it was not well characterised by the simple spectral models used in Ricci et al. (2017) or that the spectrum has a low signal-to-noise ratio.

We do not expect these selections to introduce any significant biases that would cause the observed spin distribution to deviate from the intrinsic one. Selecting based on obscuration properties and the exclusion of blazars are both expected to be related mainly to our viewing angle to these AGN (e.g. Antonucci 1993), which is not dependent on the spin of their central SMBHs. The Eddington ratio selection relates specifically to the accretion rate onto the AGN ‘today’, while the spin of the SMBH will be mainly determined by its long-term growth history instead. Indeed, the Horizon-AGN simulation shows no connection between SMBH spin and the instantaneous accretion rate in the analysed snapshot. Finally, the reflection fraction selection still permits spins across the full range of possible prograde spin values ($a^* = 0 - 0.998$), as even Schwarzschild black holes ($a^* = 0$) should result in reflection from the disc with $R \geq 1$ if the disc reaches the ISCO (e.g. Dauser et al., 2016).

Our various cuts leave a sample of 192 AGN from BASS for which spin measurements should be possible. All of these sources are relatively local, with a median redshift of $z \sim 0.05$ (see ‘BASS parent’ in the right panel of Figure 4), consistent with the $z = 0.0556$ snapshot of the Horizon-AGN simulation we use in this work. Conveniently, these sources span a broad range of black hole masses, $5.5 \lesssim \log(M_{\text{BH}}/M_{\odot}) \lesssim 10.0$, (middle and left panels in Fig. 4) which is well suited to placing constraints on different potential black hole growth models. The sample is also particularly appropriate for comparisons against Horizon-AGN specifically, with the M_{BH} distribution in our parent BASS sample showing good qualitative agreement with the black holes extracted from the cosmological simulation (left panel in Fig. 4).

7 SAMPLE SIZE AND SPIN UNCERTAINTY REQUIREMENTS

In order to design observational strategies for differentiating between supermassive black hole growth scenarios with spin parameter measurements, we need to establish the sample size and maximum spin measurement uncertainty (σ_{a^*}) necessary for such work. Both requirements are imposed by a combination of two independent factors: the difference between the SMBH growth history models as a function of mass

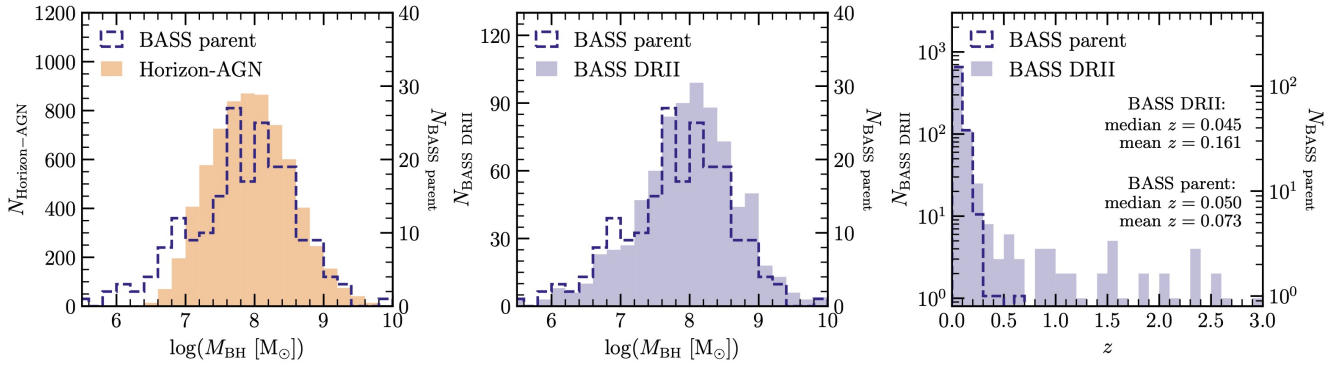


Figure 4. Left panel: comparison of SMBH mass distributions between our parent BASS sample (BASS parent, Section 6.1 and the Horizon-AGN cosmological simulation, demonstrating good agreement between potential AGN targets and the cosmological model. Middle panel: M_{BH} comparison between the whole BASS catalogue (BASS DRII) and out parent BASS sample. The distributions in M_{BH} are comparable, demonstrating that our sample selection criteria do not introduce additional bias with respect to the full BASS DRII catalogue. Right panel: comparison of redshift distributions between our parent BASS sample and the full BASS DRII AGN catalogue sources. As expected, our sample selection removes highest- z sources, however the median z remains comparable at $z \sim 0.05$.

in Horizon-AGN, and the SMBH mass distribution of our parent BASS sample (Section 6.1). In order to determine these requirements, below we simulate a set of potential survey programmes covering a range of realistic measurement uncertainties and sample sizes.

7.1 Simulating Realistic Samples Informed by Horizon-AGN

Fig. 2 shows that the two SMBH growth scenarios separate in the $M_{\text{BH}} - a^*$ plane above $10^8 M_{\odot}$, with the strongest difference at the high- M_{BH} end. It is also apparent that at high masses the accretion + mergers distribution (orange) spans a broad range in spin parameter values. Therefore, in order to differentiate between the two growth scenarios with realistic samples, we base our strategy on a simple statistical approach - discretising the spin-mass plane by calculating sample means in bins of M_{BH} . This way we can both reduce the impact of the uncertainty on individual $M_{\text{BH}} - a^*$ measurements and coarsely capture the two-dimensional trends which would otherwise require large sample sizes for a direct comparison between 2D distributions. To best capture the signal we select one bin below $M_{\text{BH}} = 10^8 M_{\odot}$ (where both scenarios make consistent predictions) and for higher masses we split the sample into two bins above and below $\log(M_{\text{BH}}/M_{\odot}) = 8.7$ ($M_{\text{BH}} \approx 5 \times 10^8 M_{\odot}$). This choice is motivated by the SMBH mass distribution shown in panel A of Fig. 4 - there are 9 AGN with $\log(M_{\text{BH}}/M_{\odot}) > 8.7$ among the brightest 100 X-ray sources in the 2-10 keV band in our parent BASS selection (which we consider as an initial plausible sample size), which yield a Poisson signal-to-noise ratio of 3 for source number count in the highest mass bin. On the low-mass end we restrict the mass bin to $M_{\text{BH}} > 10^6 M_{\odot}$ to match Horizon-AGN M_{BH} distribution. Our final binning scheme results in the following ranges in $\log(M_{\text{BH}}/M_{\odot})$: [6.0, 8.0], [8.0, 8.7] and [8.7, 10.0].

By estimating mean a^* values, we take advantage of the \sqrt{M} scaling with sample size M of the standard error on the mean, which allows us to clearly separate the two SMBH growth scenarios in the coarsely binned $M_{\text{BH}} - a^*$ plane. With M_{BH} ranges in place, we can now determine the minimum sample size and uncertainty required for a series of mean a^* measurements to differentiate between the orange and blue SMBH populations in Fig. 2. We proceed by selecting the K brightest sources from our parent BASS sample for a set of different values for K , thus imposing a single X-ray flux limit across the whole range

in SMBH mass in each case. This way we match the assumptions discussed earlier in Sec. 4 and hence can implement the radiative efficiency - spin parameter bias expected for flux-limited AGN samples in the local Universe. We then extract a^* distributions for both SMBH growth histories in each M_{BH} bin from Horizon-AGN and correct them for the $\eta(a^*)$ bias (see Appendix for details).

To simulate realistic samples of AGN, we take a total of $K = \sum K_i$ random draws from the bias-corrected spin distributions across all M_{BH} bins, with the sample sizes K_i in each individual bin determined by the number of BASS sources which fall within this SMBH mass range¹⁰, among the K brightest AGN from our selection in Sec. 6.1. We perform the spin draws separately for each SMBH growth model, and hence for each realisation of a potential observational sample of a total K AGN we have a paired set of predicted spin values for the accretion-only and accretion + mergers growth models. To simulate the effect of measurement uncertainty we then perturb the spin values drawn above by further random draws from a normal distribution $N(0, \sigma_{a^*})$, where σ_{a^*} is the assumed uncertainty on the spin measurements¹¹, for a range of values for σ_{a^*} . For each a_i^* , the normal distribution is singly truncated at $\sigma_i = (0.998 - a_i^*)/\sigma_{a^*}$ to account for the theoretical upper limit on the spin parameter of $a^* = 0.998$. This way, each potential AGN sample from a given SMBH growth history consists of K spin measurements expected from $\eta(a^*)$ bias-corrected Horizon-AGN distributions, post-processed to account for measurement uncertainty.

As a final step in each simulated AGN sample, for each mass bin we calculate the mean spin value together with its corresponding standard error on the mean: $\mu_{\text{acc}} \pm \delta_{\text{acc}}$ for the accretion-only scenario and $\mu_{\text{acc+mer}} \pm \delta_{\text{acc+mer}}$ for accretion + mergers. To calculate the standard error, we necessarily assume that each paired draw consists of a^* measurements without lower limits in both SMBH growth histories, however, we note that some are likely to be present in real observations. Finally, we check the probability of the two mean measurements in a mass bin Ω being drawn from the same underlying distribution by calculating the right-tail p-value (p_Ω) of $\mu_{\text{acc}} - \mu_{\text{acc+mer}}$ belonging to $N(0, \sqrt{\delta_{\text{acc}}^2 + \delta_{\text{acc+mer}}^2})$. This way, we calculate the probability that a given paired set of predicted spin values in a bin cannot differentiate between the accretion-only and accretion + mergers growth scenarios. For our simulated AGN samples we consider spin measurement uncertainties in the range $\sigma_{a^*} \in [0.02, 0.05, 0.10, 0.15, 0.20]$, and sample sizes of $K \in [50, 70, 100, 150, 192]$. For each combination of these values we repeat the above process 10^4 times, generating a large set of potential AGN samples, together with their corresponding mean spin parameter measurements as a function of mass.

Fig. 5 shows the fraction of these simulated AGN samples which result in a statistically different measurement of mean spin parameter value between the accretion-only and accretion+mergers SMBH growth scenarios as a function of a^* measurement uncertainty and sample size. In order to take full advantage of the difference between the two predictions at high SMBH masses, in each realisation of a potential AGN sample we combine the results for both of the mass bins with $M_{\text{BH}} > 10^8 M_\odot$. Since these can be treated as independent measurements, the combined probability of the simulated accretion-only and accretion+mergers samples being drawn from the same distribution in the $M_{\text{BH}} - a^*$ plane for *both* mass bins becomes $p_{\text{total}} = p_{[8,8.7]} \times p_{[8.7,10]}$. The vertical axis in Fig. 5 shows the fraction of simulated measurements which result in $p_{\text{total}} < 0.01$ as a function of σ_{a^*} in the x-axis. Different lines and markers correspond to the top 192, 150, 100, 70 and 50 brightest AGN in our parent BASS sample. Whenever the curves enter the gray hatched region, the median measurement expected from the 10^4 realisations

¹⁰ Throughout the study we treat the 3 sources with $M_{\text{BH}} < 10^6 M_\odot$ in the parent BASS sample as belonging to the lowest mass bin, given the large uncertainty associated with low M_{BH} estimates

¹¹ Note that at this point we simply assume all spin measurements to have the same uncertainty; more realistic scenarios that include the expected dependence of measurement uncertainties as a function of spin are considered below in Section 9.

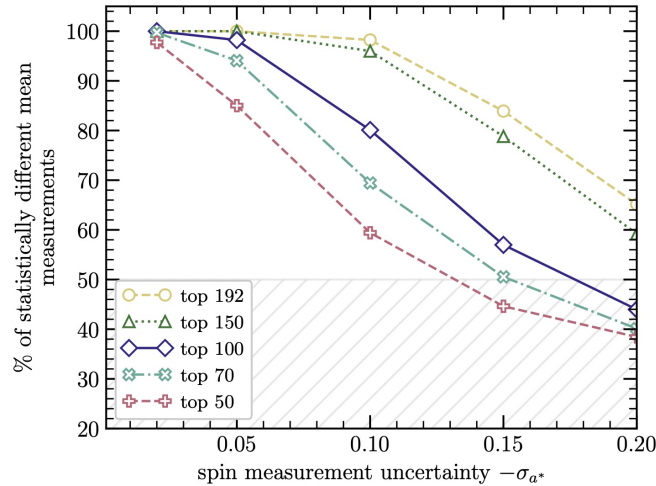


Figure 5. Minimum spin measurement uncertainty (σ_{a^*}) and sample size required for simulated observations to differentiate between accretion-only and merger & accretion SMBH growth scenarios drawn from the HorizonAGN cosmological simulation. Individual curves show the simulated observations performed for the top 50, 70, 100, 150 and 192 brightest X-ray sources in the 2-10 keV band in our parent BASS sample. In order for a median (50th percentile) simulated measurement to tell SMBH growth histories apart, one requires Gaussian spin measurement uncertainty of $\lesssim 0.15$ across the entire range in a^* for a sample of 70 sources.

of potential AGN samples will not differentiate between the accretion-only and accretion + mergers BH growth scenarios.

As expected, Fig. 5 shows that increasing the uncertainty on individual spin measurements at fixed sample size decreases the fraction of simulated samples capable of differentiating between the two SMBH growth histories. Similarly, at fixed uncertainty, a larger sample size results in higher chances for a single realisation of such a sample to tell the two growth histories apart. In the context of minimum survey requirements, we find that for a sample size of >70 AGN we would need a maximum of $\sigma_{a^*} \lesssim 0.15$ for a median expected measurement to differentiate between the accretion-only and accretion + mergers SMBH populations. In order to be conservative, we therefore suggest that a sample size of $N = 100$ AGN drawn from our BASS selection with spins measured to a precision of $\sigma_{a^*} \sim 0.15$ (or better) would be sufficient to distinguish between these different SMBH growth scenarios.

8 HEX-P SIMULATIONS

Given the importance of simultaneous broadband X-ray spectroscopy for providing observational constraints on BH spin, a mission with the profile of *HEX-P* is ideally suited to building the significant samples of SMBH spin measurements required to finally connect these measurements to cosmological BH growth models. We now present a set of simulations that showcase the anticipated capabilities of *HEX-P* in this regard.

8.1 Mission Design

The low-energy telescope (LET) onboard *HEX-P* consists of a segmented mirror assembly coated with Ir on monocrystalline silicon that achieves a half power diameter of $3.5''$, and a low-energy DEPFET detector, of the same type as the Wide Field Imager (WFI; Meidinger et al. 2020) onboard Athena (Nandra et al., 2013). It has 512×512 pixels that cover a field of view of $11.3' \times 11.3'$. It has an effective passband

of 0.2–25 keV, and a full frame readout time of 2 ms, which can be operated in a 128 and 64 channel window mode for higher count-rates to mitigate pile-up and faster readout. Pile-up effects remain below an acceptable limit of $\sim 1\%$ for fluxes up to ~ 100 mCrab in the smallest window configuration (64w). Excising the core of the PSF, a common practice in X-ray astronomy, will allow for observations of brighter sources, with a typical loss of up to $\sim 60\%$ of the total photon counts.

The HET consists of two co-aligned telescopes and detector modules. The optics are made of Ni-electroformed full shell mirror substrates, leveraging the heritage of XMM-Newton, and coated with Pt/C and W/Si multilayers for an effective passband of 2–80 keV. The high-energy detectors are of the same type as flown on *NuSTAR*, and they consist of 16 CZT sensors per focal plane, tiled 4×4 , for a total of 128×128 pixel spanning a field of view of $13.4' \times 13.4'$.

8.2 Instrumental Responses

All the mission simulations presented here were produced with a set of response files that represent the observatory performance based on current best estimates (see [Madsen et al. 2023]). The effective area is derived from raytracing calculations for the mirror design including obscuration by all known structures. The detector responses are based on simulations performed by the respective hardware groups, with an optical blocking filter for the LET and a Be window and thermal insulation for the HET. The LET background was derived from a GEANT4 simulation (Eraerds et al., 2021) of the WFI instrument, and the one for the HET from a GEANT4 simulation of the *NuSTAR* instrument, both positioned at L1. The broad X-ray passband and superior sensitivity will provide a unique opportunity to study accretion onto SMBHs across a wide range of energies, luminosities, and dynamical regimes.

8.3 Spectral Simulations

To assess the ability of *HEX-P* to constrain black hole growth models via AGN spin measurements, we perform a series of spectral simulations covering a range of spin values relevant to the cosmological simulations discussed above: $a^* = 0.5, 0.7, 0.9, 0.95$. We first focus on the lowest spin value among this set, $a^* = 0.5$, and perform a set of simulations at different exposures in the range 50–200 ks. For each exposure, we simulate 100 different spectra using the above response files and the XSPEC spectral fitting package (v12.11.1; Arnaud 1996), in order to determine the minimum exposure that provides the *HEX-P* data quality needed for an average 1σ constraint on the spin of $\sigma_{a^*} \leq 0.15$, as required above. We then perform further sets of 100 simulations with this exposure for each of the spin values listed above to map out the expected uncertainty as a function of input spin (as it is now well-established that for a given observational setup tighter constraints can be obtained for higher spin values, e.g. Bonson and Gallo 2016; Choudhury et al. 2017; Kammoun et al. 2018; Barret and Cappi 2019).

We make use of the RELXILL family of disk reflection models (García et al. 2014; Dauser et al. 2014) for these simulations, and construct a spectral model that draws on the typical properties of the ~ 200 BASS AGN selected above (Section 6.1), general expectations for the unobscured AGN selected based on the unified model for AGN, and typical results seen from AGN for which detailed reflection studies have already been possible in the literature. We specifically make use of the RELXILLPCP model, which assumes a simple lamppost geometry for the corona, and that the ionising continuum is a thermal Comptonization model (specifically the NTHCOMP model; Zdziarski et al. 1996; Zycki et al. 1999).

For the key model parameters, we assume the spectrum of the primary continuum has parameters $\Gamma = 2.0$ and $kT_e = 100$ keV for the photon index and electron temperature, respectively, relatively typical parameters for unobscured AGN (Ricci et al. 2017; Baloković et al. 2020). This illuminates a geometrically

thin accretion disk which is assumed to extend down to the ISCO. AGN with moderate-to-low levels of obscuration are generally expected to be viewed at moderate-to-low inclinations in the unified model (Antonucci 1993), so we assume an inclination of 45° . The disk is assumed to be ionised, with an ionisation parameter¹² of $\log[\xi/(\text{erg cm s})] = 2$ (typical of values reported from relativistic reflection analyses in the literature, e.g. Ballantyne et al. 2011; Walton et al. 2013; Jiang et al. 2019; Mallick et al. 2022), and to have solar iron abundance of (i.e. $A_{\text{Fe}} = 1$). We assume the corona has a height of $5 R_G$ for the $a^* = 0.5$ simulations, and then that it has constant height in vertical horizon units as we subsequently vary the spin. This is equivalent to assuming the scale of the corona contracts slightly as the inner radius of the disk moves inwards, as might be expected should the corona be related to magnetic re-connection around the inner disk (e.g. Merloni and Fabian 2001); in gravitational radii these coronal heights correspond to values in the range $\sim 4\text{--}5 R_G$, which are relatively standard values inferred for the sizes of X-ray coronae (e.g. Reis and Miller 2013; De Marco et al. 2013; Kara et al. 2016; Mallick et al. 2021). The reflection fraction is calculated self-consistently based on the combination of a^* and h , both when computing the simulations and also when subsequently fitting the simulated data to explore the constraints on a^* .

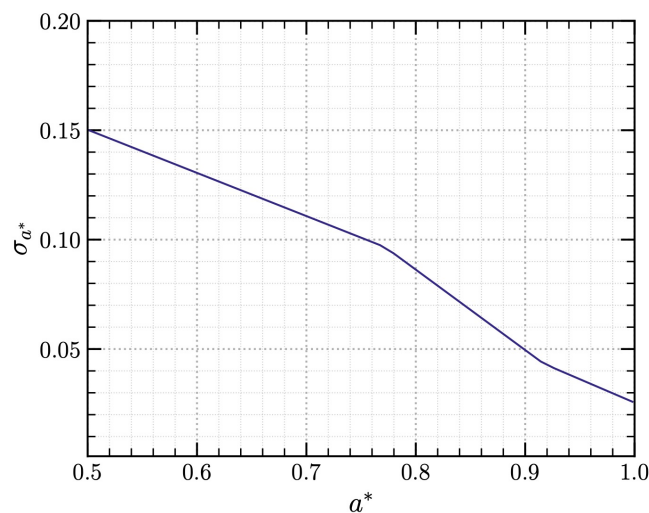


Figure 6. Spin parameter measurement uncertainty $\sigma(a^*)$ vs spin parameter a^* , extracted from the *HEX-P* spectral simulations of relativistic reflection in AGN discussed in Section 8.3 (which assume a 2–10 keV flux of $6 \times 10^{-12} \text{ erg cm}^{-2} \text{ s}^{-1}$ and an exposure time of 150 ks).

As we need a sample of ~ 100 AGN to distinguish the black hole growth models, we normalise all of our simulations to have a 2–10 keV flux of $6 \times 10^{-12} \text{ erg cm}^{-2} \text{ s}^{-1}$, as this is the flux of the 100th brightest source in the sample of AGN selected above (see Section 6.1). At this flux level, we find that a *HEX-P* exposure of 150 ks is required to provide an average uncertainty of $\sigma_{a^*} \leq 0.15$ for an input spin value of $a^* = 0.5$. We also find that, as broadly expected, the typical uncertainty on the spin measurements *HEX-P* will decrease for more rapidly rotating black holes (see Figure 6). Although our results do differ quantitatively to the prior efforts that have also come to similar conclusions, the overall quantitative trend we find is consistent with these previous works (e.g. Bonson and Gallo 2016; Kammoun et al. 2018). These quantitative differences mainly relate to the fact that we are simulating *HEX-P* spectra instead of *XMM-Newton+NuSTAR* spectra, with some contribution from the fact that different model versions and

¹² The ionisation parameter has its usual definition of $\xi = L/nR^2$, where L is the ionising luminosity, n is the number density of the plasma, and R is the distance between the plasma and the ionising source.

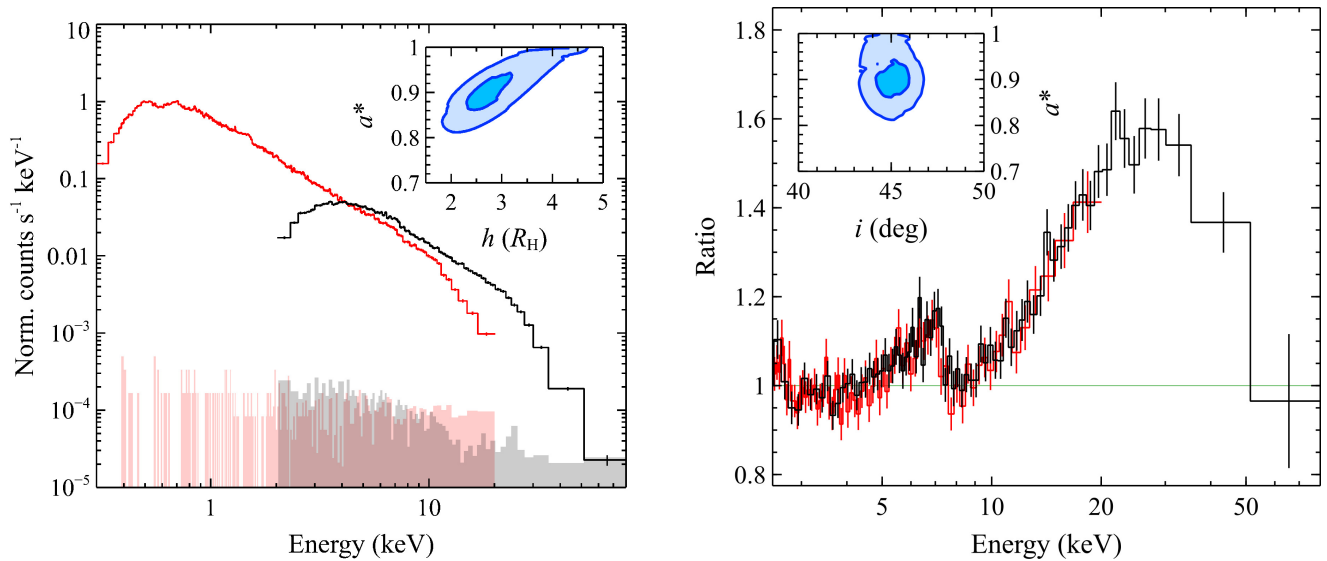


Figure 7. *Left panel:* Count spectra for the LET (red) and the combined HET (black) for one of our *HEX-P* spectral simulations with $a^* = 0.9$, along with their corresponding instrumental backgrounds (shaded regions). *Right panel:* The same simulated spectra plotted as a ratio to a simple CUTOFFPL continuum model (a powerlaw with an exponential high-energy cutoff), fit to the 2–4, 8–10 and 50–80 keV bands (where the primary continuum would be expected to dominate). We zoom in on the data above 2 keV to highlight the key reflection features: the relativistically broadened Fe $K\alpha$ peaking at ~ 6 –7 keV and the Compton hump peaking at ~ 30 keV. The two insets show the projected constraints on a^* , h and i for this simulation (displayed as 2-D confidence contours, with the 1σ and 2σ levels shown).

slightly different assumptions are used here. An example spectrum from one of our simulations for $a^* = 0.9$ is shown in Figure 7, along with the projected constraints on a^* , i and h for that simulation.

9 CONSTRAINING SMBH GROWTH CHANNELS WITH *HEX-P*

Having established both the minimum survey requirements and the *HEX-P* S/N that will be required to meet these, we now demonstrate the mission’s ability to differentiate between accretion-only and accretion + mergers supermassive black hole growth scenarios. To this end we repeat the simulations introduced earlier in Sec. 7.1 for the brightest 100 sources in our parent BASS sample (Sec. 6.1), this time replacing the constant spin parameter uncertainty σ_{a^*} assumed previously with the a^* -dependent uncertainties $\sigma(a^*)$ obtained from spectral simulations in Sec. 8.3 (see Fig. 6), i.e. now specifically simulating observational campaigns with *HEX-P*. Similarly to our initial tests, we simulate 10^4 paired AGN samples to assess the probability with which *HEX-P* will confidently discriminate between SMBH growth histories.

Fig. 8 illustrates the observational constraints that would be expected for one such paired set of simulated AGN samples, randomly selected from our set of such simulations, comparing the accretion-only (blue circles) and accretion + mergers (orange squares) SMBH growth scenarios against the current spin parameter constraints for $M_{\text{BH}} > 10^6 M_{\odot}$ (grey diamonds). In order to account for the existence of lower limits expected in realistic measurements, by analogy with the measurements collected from the literature, we use open symbols to indicate right-censored spin draws, i.e. a_i^* for which $0.998 - a_i^* < \sigma(a_i^*)$. Vertical error bars mark 1σ uncertainties in both simulated and existing $M_{\text{BH}} - a^*$ constraints, allowing for a direct comparison between the two. All BASS M_{BH} measurements in the figure are assigned a ± 0.3 dex uncertainty expected for their estimate via the $M_{\text{BH}} - \sigma_*$ relation (Kormendy and Ho, 2013). Fig. 8 clearly

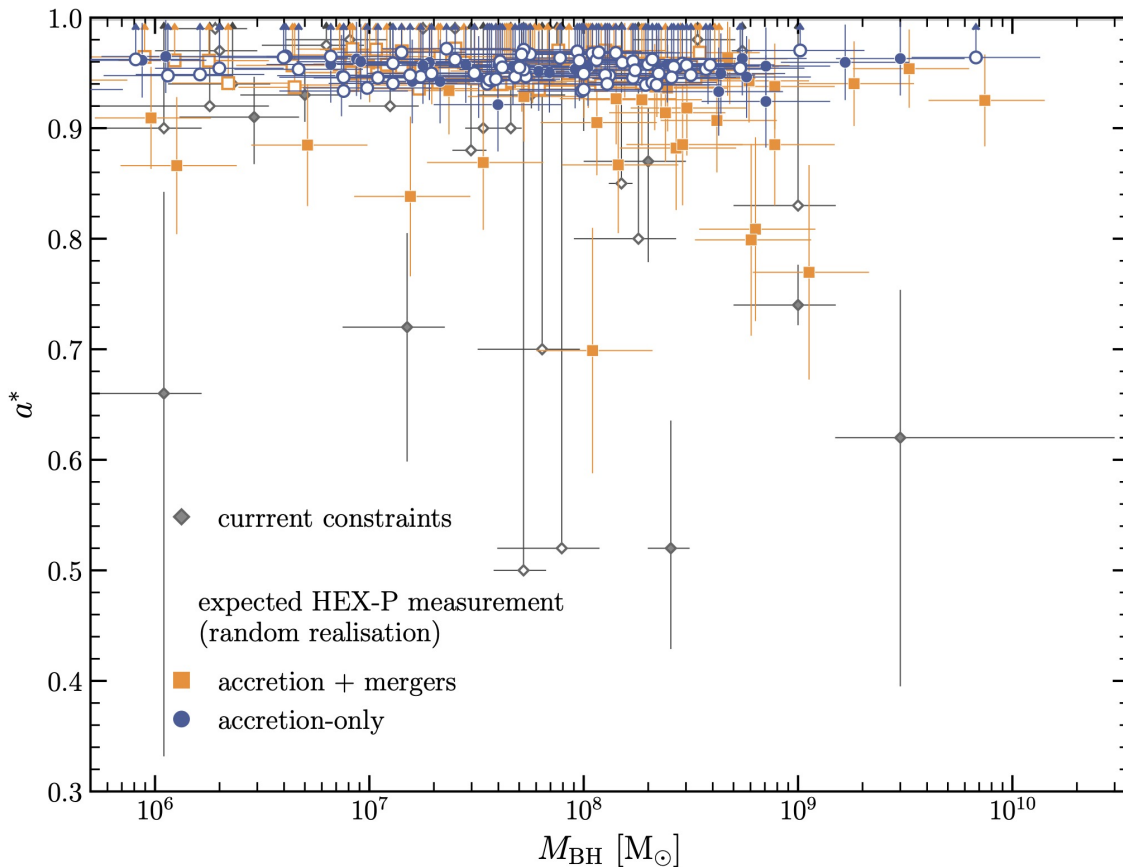


Figure 8. Comparison between current published constraints (grey diamonds) and a random realisation of simulated *HEX-P* measurements for the accretion-only (blue circles) and accretion + mergers SMBH growth scenarios (orange squares). Empty symbols show lower limits on a^* , while filled symbols denote measurements with vertical errorbars marking their corresponding 1σ confidence ranges. With its expected spin measurement uncertainty *HEX-P* will provide unprecedented constraints on the $M_{\text{BH}} - a^*$ plane for SMBH in the local Universe.

demonstrates the potential for such a *HEX-P* spin measurement campaign to map the spin-mass plane with unprecedented accuracy. In comparison with currently available constraints, the *simulated observations* offer visible improvements on measurement precision, good control of sample selection biases and an over twofold increase in sample size.

Moving on from an individual realisation, the top panels in Fig. 9 present the distribution of mean a^* measurements (μ) for the whole suite of 10^4 simulations for the accretion + mergers (orange) and accretion-only (blue) SMBH growth histories for the three bins of M_{BH} . Vertical dashed lines mark μ at which each distribution peaks, indicating the most likely expected mean spin parameter measurement for each growth scenario. Similarly, bottom panels present the corresponding distributions of the standard errors on the mean (δ) together with their peaks marked with vertical dashed lines. The mean spin parameter values from Horizon-AGN together with their most likely measurements expected from *HEX-P* observations are summarised in Table 1.

Table 1. Summary of mean spin parameter values in simulated *HEX-P* observations and Horizon-AGN

log(M_{BH}/M_{\odot}) bin		[6.0, 8.0]	[8.0, 8.7]	[8.7, 10.0]
Horizon-AGN	accretion-only	0.996	0.993	0.993
	accretion + mergers	0.959	0.905	0.768
Horizon-AGN with $\eta(a^*)$ bias	accretion-only	0.996	0.995	0.995
	accretion + mergers	0.981	0.953	0.851
Expected measurement	accretion-only	0.977 ± 0.002	0.975 ± 0.003	0.976 ± 0.005
	accretion + mergers	0.966 ± 0.004	0.945 ± 0.011	0.86 ± 0.04

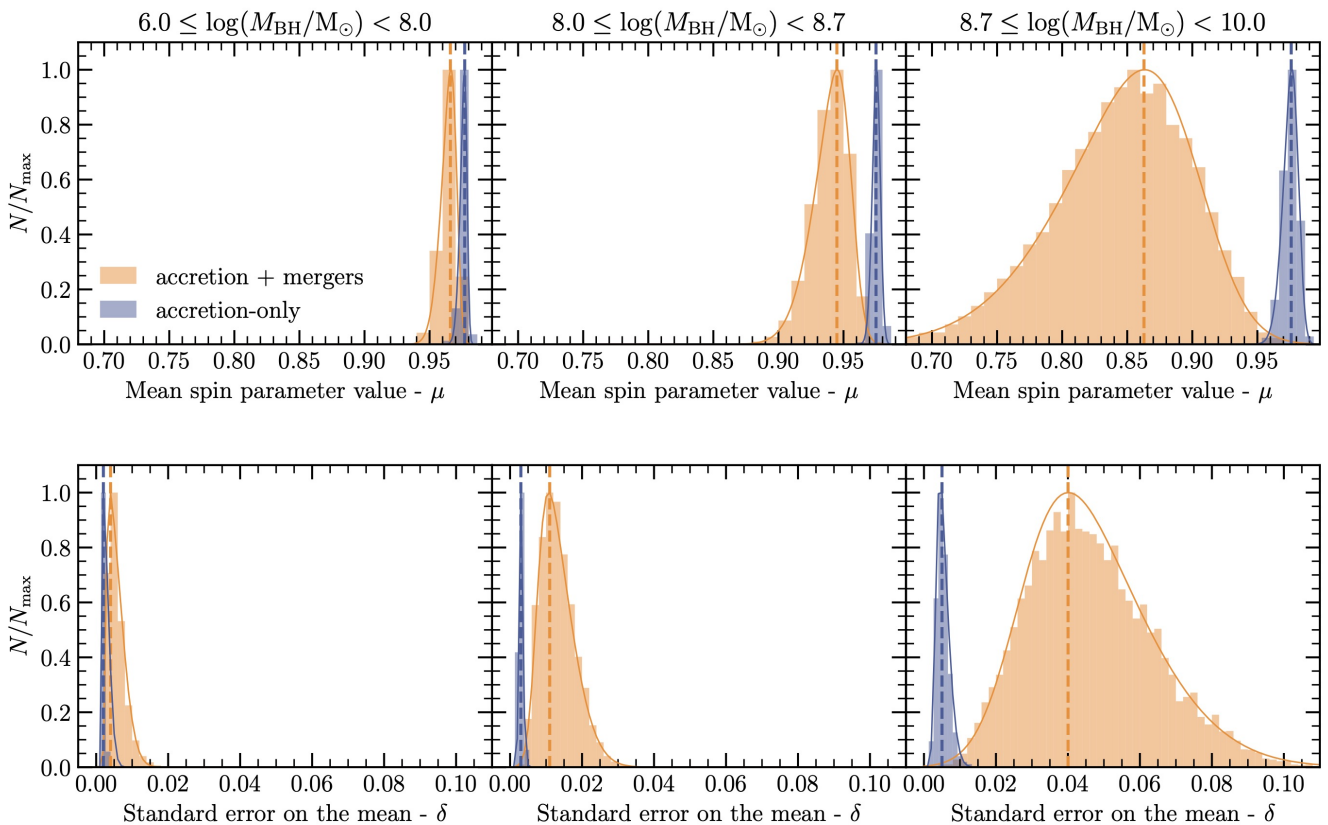


Figure 9. Summary of mean spin parameter estimates for 10^4 realisations of simulated *HEX-P* observing campaigns. *Top panels:* distribution of expected mean a^* estimates (μ) in bins of M_{BH} for accretion-only (blue) and accretion + mergers (orange) SMBH growth scenarios. *Bottom panels:* corresponding distributions of the standard errors on the mean (δ). Peak locations in each distribution are marked with vertical dashed lines. Differences between the mean spin measurements for the two scenarios become apparent for $M_{\text{BH}} > 10^8 M_{\odot}$ with the most massive bin showing the strongest signal.

Together Fig. 9 and Table 1 demonstrate the potential of mean a^* measurements in bins of M_{BH} for differentiating between the accretion-only and accretion + mergers SMBH growth scenarios within the Horizon-AGN cosmological model. As expected from Fig. 2, the simulated constraints in the lowest mass bin are consistent between the two SMBH populations, but become statistically separable for $M_{\text{BH}} > 10^8 M_{\odot}$. In all three panels in Fig 9, μ_{acc} distributions are narrower than in the accretion + mergers case, with consistently high peak values matching the true $\eta(a^*)$ bias-corrected mean a^* in Horizon-AGN to

within $< 2\%$. The orange distributions, on the other hand, peak at progressively lower $\mu_{\text{acc+mer}}$ values with increasing M_{BH} , following the trend expected from the cosmological simulation to within $< 2\%$ as well. We also note that the simulated accretion + mergers mean spin measurements form a visibly left-skewed distribution primarily owing to the progressive spin parameter uncertainty prescription in our simulations, which assumes larger σ_{a^*} for lower spin values based on our *HEX-P* spectral simulations (Section 8.3)¹³. The middle mass bin shows a non-negligible overlap between the μ_{acc} and $\mu_{\text{acc+mer}}$ distributions, however their two peaks are clearly separated by $\Delta\mu \simeq 0.03$. For $\log(M_{\text{BH}}/M_{\odot}) > 8.7$ the two SMBH growth scenarios form virtually non-overlapping distributions with peak μ separated by $\Delta\mu \simeq 0.16$, despite the modest number of 9 BASS sources available in the mass bin. We note, however, that small sample statistics do lead to a significant spread in the simulated $\mu_{\text{acc+mer}}$ values.

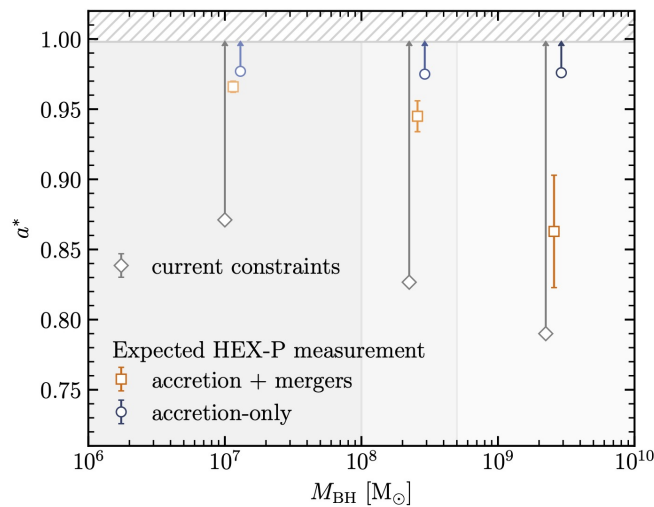


Figure 10. Comparison of mean spin parameter measurements in bins of M_{BH} between published constraints (grey diamonds) and expected HEX-P measurements for accretion-only (blue circles) and accretion + mergers (orange squares) SMBH growth scenarios. For HEX-P measurements we show the most likely result from our simulations, corresponding to the vertical dashed lines in Fig. 9. Background shading marks our M_{BH} binning scheme, while the grey hatching at the top indicates spin parameter range forbidden by Thorne (1974) limit. The expected *HEX-P spin parameter measurements will allow us to differentiate between SMBH growth histories*, unlike $M_{\text{BH}} - a^*$ constraints placed until now.

In Fig. 10 we summarise the prospects for constraining the cosmic growth history of supermassive black holes via X-ray reflection spectroscopy with a *HEX-P* spin survey similar to the design outlined above. The figure shows the expected mean a^* measurements in three bins of M_{BH} for accretion-only (blue circles) and accretion + mergers (orange squares) scenarios, inferred from our suite of simulated observations of the brightest 100 AGN in our parent BASS sample. The y -axis locus of individual points correspond to the vertical dashed lines in the top panels of Fig. 9, while the length of the error bars correspond to the vertical dashed lines in the bottom panels. Since it is likely that observations of high- a^* SMBHs will result in a significant fraction of constraints that are lower limits, we mark the prediction for the accretion-only growth scenario as a lower limit. We also compare the results of our simulations to the current constraints, showing mean spin parameter values in identical mass bins for $M_{\text{BH}} - a^*$ measurements calculated earlier in Section 4.1 (and presented earlier in Fig 2).

¹³ The skewness is also present in the accretion-only scenario, however this effect is more not so visibly apparent due to the narrow width of the distribution.

Fig. 10 clearly demonstrates that *future HEX-P spin measurements will allow us to differentiate between the two SMBH growth channels as inferred from the Horizon-AGN cosmological model*. The expected mean measurements in the highest mass bin alone reject the null hypothesis of the accretion-only and accretion + mergers results being drawn from the same distribution at the level of 2.8σ ($p_{[8.7-10.0]} = 2.5 \times 10^{-3}$). Across the whole suite of our simulations, $> 82\%$ ($> 36\%$) of paired simulated measurements in the highest mass bin reject the null hypothesis at $> 2\sigma$ ($> 3\sigma$) confidence level. When we combine the measurements for both mass bins above $10^8 M_\odot$ in SMBH mass, the expected *HEX-P* measurement can differentiate between the two growth histories at $\sim 4.3\sigma$ and across all simulated measurements at $> 3\sigma$ ($> 4\sigma$) confidence level in $> 88\%$ ($> 65\%$) of all paired draws. Fig. 10 also illustrates that the current spin constraints are not yet sufficient to make the distinction between these different growth scenarios; a dedicated SMBH spin survey with improved individual constraints, a larger sample size and well-controlled biases – similar to the one envisioned here for *HEX-P* – is really needed to drive the combined SMBH spin constraints to the level that they are able to do so.

10 FINAL REMARKS

We have now confirmed that a sample of 100 AGN with the data quality determined in Section 7 and the mass distribution of the 100 brightest sources in our BASS selection (Section 6.1) should be sufficient to distinguish between different cosmological SMBH growth scenarios. Moving on, we finish our analysis with an assessment of the level of observational investment from *HEX-P* that would be required to achieve this result. Given that a 150 ks *HEX-P* exposure provides the necessary data quality for our required spin constraints ($\sigma_{a^*} \leq 0.15$ for $a^* = 0.5$) for a source with a 2–10 keV flux of 6×10^{-12} erg cm $^{-2}$ s $^{-1}$, we calculate a rough estimate for how long it would take for *HEX-P* to provide this level of data quality for all of these 100 sources by scaling this 150 ks exposure to the actual observed 2–10 keV flux for each source (also reported in the BASS catalogue). Formally this is a slightly conservative approach, as the instrumental background will make a smaller contribution for higher source fluxes. Even then, for the faintest of these sources the background already only impacts the highest energies probed by each detector (see Figure 7), so the *HEX-P* background is likely low enough to only have a minimal effect across this sample. Summing the exposure required for each of the brightest 100 sources, we find that a total observing investment of ~ 10 Ms from *HEX-P* would be necessary.

While this is undoubtedly a very significant investment, it is nevertheless a program that would be achievable when spread over the full 5-year lifetime of *HEX-P*. In particular, a spin survey such as this could serve a similar function to the *HEX-P* mission as the ongoing *Swift*/BAT survey conducted by *NuSTAR* (e.g. Baloković et al. 2020). This program gradually builds up *NuSTAR* observations of hard X-ray sources detected by the *Swift*/BAT detector via regular scheduling of short ‘filler’ observations, which are easily around the more extensive Guest Observer program. Indeed, even the longest exposures required here – 150 ks – could be split into 3×50 ks observations for ease of scheduling. The regular inclusion of such observations in the schedule would also allow for increased flexibility regarding the ability of *HEX-P* to respond to transient phenomena (i.e. target-of-opportunity observations), as these survey observations can easily be rescheduled, since they have no real time constraints and the simultaneity of the coverage across the full 0.3–80 keV bandpass is already guaranteed.

Most importantly, our study demonstrates that in the light of theoretical predictions delivered by state-of-the-art cosmological hydrodynamical simulations tracing SMBH spin evolution, only large statistical samples of consistent measurements are capable of isolating SMBH growth channels. Once radiative efficiency-spin bias is accounted for, the differences in statistical properties of SMBH populations in

the $M_{\text{BH}} - a^*$ plane decrease in magnitude, requiring both high precision on individual measurements and numerous AGN observations at $M_{\text{BH}} > 10^8 M_{\odot}$ to constrain average trends in spin parameter as a function of SMBH mass. Although such measurements are, in principle, possible with currently available instruments, they critically require simultaneous observations with soft and hard X-ray observatories (e.g. *XMM-Newton* and *NuSTAR*). The necessary exposure time comparable to the expected *HEX-P* investment for these observatories renders such a study simply unfeasible, due to the limitations associated with program allocation and scheduling conflicts among individual instruments.

Beyond distinguishing cosmological BH growth scenarios via the spin measurements, the high-S/N broadband X-ray data generated by such a survey would represent an undoubted legacy for the *HEX-P* mission, and broader studies of AGN in general. For example, inner disk inclinations will be well constrained (see Fig. 7), providing further tests of the broad applicability of the Unified Model (Antonucci 1993) as well as allowing for additional sanity checks of the reflection results/searches for disk warps via comparison of these inclinations with constraints from the outer disk from e.g. VLT/GRAVITY (see the cases of NGC3783 and IRAS 09149-2461, where the inner and outer disk inclinations from reflection studies and GRAVITY are in excellent agreement: Brenneman et al. 2011; Walton et al. 2020; GRAVITY Collaboration et al. 2020, 2021). These observations would also provide good constraints on the X-ray corona for a large sample of AGN, both in terms of its size scale (see Figure 7) and its plasma physics via temperature measurements; all of these observations will allow for good constraints on the electron temperature, facilitating further tests of coronal models (e.g. Fabian et al. 2015; see also [Kammoun et al. 2023]). All-in-all, while a program of this nature would be a major investment, the scientific return provided would be suitably vast.

11 APPENDIX

11.1 Radiative efficiency – spin bias in flux limited samples

A strong, positive, nonlinear relationship between the black hole spin parameter and the radiative efficiency in thin relativistic disks (Novikov and Thorne, 1973) is frequently discussed in the literature as a potential source of observational bias for SMBH spin measurements, preferentially selecting sources with higher a^* . In order to account for this bias in our predictions from the Horizon-AGN cosmological simulation, we consider the effect this $\eta(a^*) - a^*$ relation has on a sample of X-ray measurements defined by a minimum observable flux (i.e. a flux-limited sample). Following the discussion in Brenneman et al. (2011), we assume that potentially observable AGN are uniformly distributed within a Cartesian space (an assumption appropriate for the low-redshift Universe probed by our parent sample of BASS sources in Section 6.1), their spin parameter a^* is independent of the instantaneous accretion rate \dot{M} and the X-ray spectra do not vary dramatically as a function of either \dot{M} or a^* .

Under these assumptions, for a given luminosity $L = \eta(a^*)\dot{M}c^2$, an X-ray flux limit effectively corresponds to a limit in distance in a Cartesian space (r_L), i.e:

$$r_L = \left(\frac{L}{4\pi F} \right)^{1/2} \propto \left(\frac{L}{F_X} \right)^{1/2}. \quad (1)$$

The total number of AGN in a given range of luminosity $L + dL$ and spin parameter $a^* + da^*$ is then given by:

$$dN = V_L \Phi(L, a^*) dL da^*, \quad \text{where} \quad V_L = \frac{4}{3} \pi r_L^3 \quad (2)$$

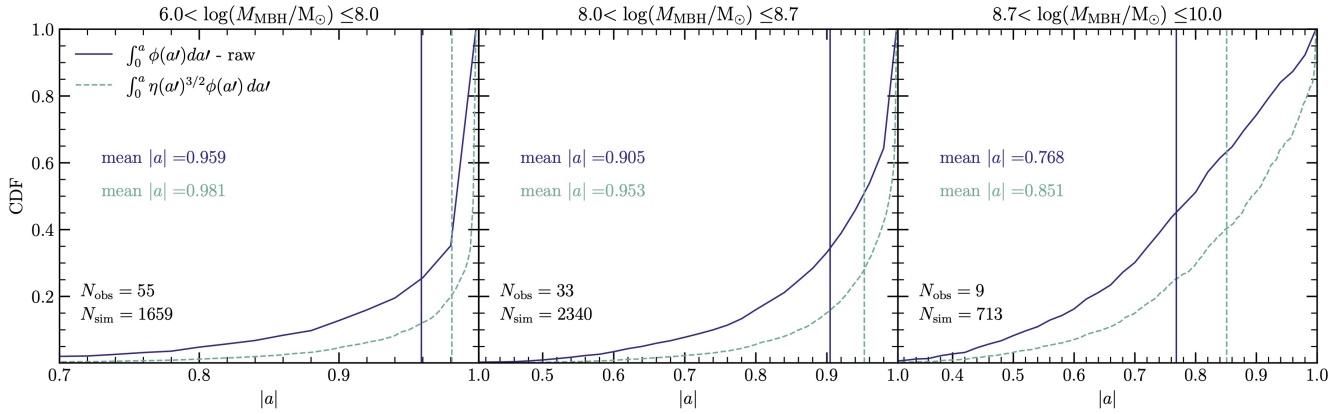


Figure 11. Change in the inferred cumulative distribution function (CDF) and associated mean a^* of the accretion + mergers Horizon-AGN SMBH population in response to the $\eta - a^*$ bias. Solid lines show the raw CDF in each M_{BH} bin, while the dashed ones indicate the CDF resulting from $\eta - a^*$ correction. Vertical solid and dashed lines indicate inferred population means for the raw and η -bias corrected distributions, respectively. Once the relationship between radiative efficiency and spin is accounted for, inferred spin distributions are shifted towards higher a^* values with the change most apparent in the highest mass bin.

and $\Phi(L, a^*)dLda^*$ is the spatial density of objects in the luminosity and spin increments. Combining Eq. 1 and 2, the number of AGN in an incremental range in a^* and L then has the following dependence on luminosity in a flux-limited sample:

$$dN \propto L^{3/2} \Phi(L, a^*)dLda^* \quad (3)$$

which from $L = \eta(a^*)\dot{M}c^2$ has the following dependency on $\eta(a^*)$ and \dot{M} :

$$dN \propto \eta(a^*)^{3/2} \dot{M}^{3/2} \Phi(\dot{M}, a^*)d\dot{M}da^*. \quad (4)$$

Assuming that \dot{M} and a^* are not mutually dependent, one can separate Φ into a product of unary functions of \dot{M} and a^* , namely $\Phi(\dot{M}, a^*) = f(a^*)g(\dot{M})$. This way, Eq. 4 becomes

$$dN \propto \eta(a)^{3/2} f(a)da \dot{M}^{3/2} g(\dot{M})d\dot{M}. \quad (5)$$

Finally, once we assume the dependence of dN on \dot{M} can be marginalised over, the total number of AGN expected per a^* increment, $dN(a^*) = \text{PDF}(a^*)$, can be expressed as

$$dN(a^*) \propto \eta(a)^{3/2} f(a^*)da^* \int_{\Omega_{\dot{M}}} \dot{M}^{3/2} g(\dot{M})d\dot{M} \quad (6)$$

and hence the final effect of the black hole spin dependence of radiative efficiency on the the cumulative distribution function of the expected spin measurements, $\text{CDF}(a^*)$, becomes:

$$\text{CDF}(a^*) = \int_0^{a^*} dN(a')da' = \int_0^{a^*} \eta(a')^{3/2} f(a')da' \quad (7)$$

Fig. 11 presents the effect of this radiative efficiency-spin bias on spin parameter distributions in the accretion + mergers SMBH population, inferred from the Horizon-AGN cosmological simulation. All

three panels compare the raw cumulative distribution functions, $CDF(a^*)$, in solid blue lines against their expected observed counterparts from flux-limited surveys in teal dashed lines. The solid and dashed vertical lines correspond to their respective mean spin parameter values. The figure is separated into three panels, showing the expected CDF in the three SMBH mass bins introduced in Sec. 7, together with black hole population sizes in each bin expected from the brightest 100 BASS AGN in our parent sample, N_{obs} , compared against the corresponding number of SMBH found in Horizon-AGN, N_{sim} . Fig. 11 clearly demonstrates how accounting for the relationship between the radiative efficiency and spin shifts the expected spin parameter distributions towards higher a^* values, biasing the expected mean a^* measurement upwards by up to $\Delta a^* = 0.083$ in the most massive bin.

CONFLICT OF INTEREST STATEMENT

The authors declare that the research was conducted in the absence of any commercial or financial relationships that could be construed as a potential conflict of interest.

FUNDING

J.M.P. and J.A.G. acknowledge support from NASA grants 80NSSC21K1567 and 80NSSC22K1120. The work of D.S. was carried out at the Jet Propulsion Laboratory, California Institute of Technology, under a contract with NASA. C.R. acknowledges support from the Fondecyt Regular (grant 1230345) and ANID BASAL (project FB210003). L.M. acknowledges support from the CITA National Fellowship.

ACKNOWLEDGMENTS

REFERENCES

- Alexander, D. M. and Hickox, R. C. (2012). What drives the growth of black holes? *New Astronomy Reviews* 56, 93–121. doi:10.1016/j.newar.2011.11.003
- Alston, W. N., Fabian, A. C., Kara, E., Parker, M. L., Dovciak, M., Pinto, C., et al. (2020). A dynamic black hole corona in an active galaxy through X-ray reverberation mapping. *Nature Astronomy* 4, 597–602. doi:10.1038/s41550-019-1002-x
- Annuar, A., Gandhi, P., Alexander, D. M., Lansbury, G. B., Arévalo, P., Ballantyne, D. R., et al. (2015). NuSTAR Observations of the Compton-thick Active Galactic Nucleus and Ultraluminous X-Ray Source Candidate in NGC 5643. *ApJ* 815, 36. doi:10.1088/0004-637X/815/1/36
- Antonucci, R. (1993). Unified models for active galactic nuclei and quasars. *ARA&A* 31, 473–521. doi:10.1146/annurev.aa.31.090193.002353
- Arévalo, P., Bauer, F. E., Puccetti, S., Walton, D. J., Koss, M., Boggs, S. E., et al. (2014). The 2-79 keV X-Ray Spectrum of the Circinus Galaxy with NuSTAR, XMM-Newton, and Chandra: A Fully Compton-thick Active Galactic Nucleus. *ApJ* 791, 81. doi:10.1088/0004-637X/791/2/81
- Arnaud, K. A. (1996). XSPEC: The First Ten Years. In *Astronomical Data Analysis Software and Systems V*, ed. G. H. Jacoby & J. Barnes. vol. 101 of *Astron. Soc. Pac. Conference Series, Astron. Soc. Pac., San Francisco*, 17
- Athanassoula, E., Bienayme, O., Martinet, L., and Pfenniger, D. (1983). Orbits as building blocks of a barred galaxy model. *A&A* 127, 349–360
- Avara, M. J., McKinney, J. C., and Reynolds, C. S. (2016). Efficiency of thin magnetically arrested discs around black holes. *MNRAS* 462, 636–648. doi:10.1093/mnras/stw1643

- Ballantyne, D. R., McDuffie, J. R., and Rusin, J. S. (2011). A Correlation between the Ionization State of the Inner Accretion Disk and the Eddington Ratio of Active Galactic Nuclei. *ApJ* 734, 112. doi:10.1088/0004-637X/734/2/112
- Baloković, M., Harrison, F. A., Madejski, G., Comastri, A., Ricci, C., Annuar, A., et al. (2020). NuSTAR Survey of Obscured Swift/BAT-selected Active Galactic Nuclei. II. Median High-energy Cutoff in Seyfert II Hard X-Ray Spectra. *ApJ* 905, 41. doi:10.3847/1538-4357/abc342
- Bambi, C. (2017). *Black Holes: A Laboratory for Testing Strong Gravity*. doi:10.1007/978-981-10-4524-0
- Bambi, C., Brenneman, L. W., Dauser, T., García, J. A., Grinberg, V., Ingram, A., et al. (2021). Towards Precision Measurements of Accreting Black Holes Using X-Ray Reflection Spectroscopy. *Space Science Reviews* 217, 65. doi:10.1007/s11214-021-00841-8
- Barausse, E. and Rezzolla, L. (2009). Predicting the Direction of the Final Spin from the Coalescence of Two Black Holes. *ApJ* 704, L40–L44. doi:10.1088/0004-637X/704/1/L40
- Bardeen, J. M. (1970). Kerr Metric Black Holes. *Nat* 226, 64–65. doi:10.1038/226064a0
- Bardeen, J. M., Press, W. H., and Teukolsky, S. A. (1972). Rotating Black Holes: Locally Nonrotating Frames, Energy Extraction, and Scalar Synchrotron Radiation. *ApJ* 178, 347–370. doi:10.1086/151796
- Barnes, J. E. and Hernquist, L. (1992). Dynamics of interacting galaxies. *ARA&A* 30, 705–742. doi:10.1146/annurev.aa.30.090192.003421
- Barret, D. and Cappi, M. (2019). Inferring black hole spins and probing accretion/ejection flows in AGNs with the Athena X-ray Integral Field Unit. *A&A* 628, A5. doi:10.1051/0004-6361/201935817
- Barthelmy, S. D., Barbier, L. M., Cummings, J. R., Fenimore, E. E., Gehrels, N., Hullinger, D., et al. (2005). The Burst Alert Telescope (BAT) on the SWIFT Midex Mission. *Space Science Reviews* 120, 143–164. doi:10.1007/s11214-005-5096-3
- Beckmann, R. S., Devriendt, J., Slyz, A., Peirani, S., Richardson, M. L. A., Dubois, Y., et al. (2017). Cosmic evolution of stellar quenching by AGN feedback: clues from the Horizon-AGN simulation. *MNRAS* 472, 949–965. doi:10.1093/mnras/stx1831
- Beckmann, R. S., Smethurst, R. J., Simmons, B. D., Coil, A., Dubois, Y., Garland, I. L., et al. (2023). Supermassive black holes in merger-free galaxies have higher spins which are preferentially aligned with their host galaxy. *MNRAS* doi:10.1093/mnras/stad1795
- Berti, E. and Volonteri, M. (2008). Cosmological Black Hole Spin Evolution by Mergers and Accretion. *ApJ* 684, 822–828. doi:10.1086/590379
- Blandford, R. D. and McKee, C. F. (1982). Reverberation mapping of the emission line regions of Seyfert galaxies and quasars. *ApJ* 255, 419–439. doi:10.1086/159843
- Blandford, R. D. and Znajek, R. L. (1977). Electromagnetic extraction of energy from Kerr black holes. *MNRAS* 179, 433–456. doi:10.1093/mnras/179.3.433
- Bondi, H. (1952). On spherically symmetrical accretion. *MNRAS* 112, 195. doi:10.1093/mnras/112.2.195
- Bondi, H. and Hoyle, F. (1944). On the mechanism of accretion by stars. *MNRAS* 104, 273. doi:10.1093/mnras/104.5.273
- Bonson, K. and Gallo, L. C. (2016). How well can we measure supermassive black hole spin? *MNRAS* 458, 1927–1938. doi:10.1093/mnras/stw466
- Bower, R. G., Benson, A. J., Malbon, R., Helly, J. C., Frenk, C. S., Baugh, C. M., et al. (2006). Breaking the hierarchy of galaxy formation. *MNRAS* 370, 645–655. doi:10.1111/j.1365-2966.2006.10519.x
- Brenneman, L. W. and Reynolds, C. S. (2006). Constraining Black Hole Spin via X-Ray Spectroscopy. *ApJ* 652, 1028–1043. doi:10.1086/508146
- Brenneman, L. W., Reynolds, C. S., Nowak, M. A., Reis, R. C., Trippe, M., Fabian, A. C., et al. (2011). The Spin of the Supermassive Black Hole in NGC 3783. *ApJ* 736, 103. doi:10.1088/0004-637X/736/2/103

- Brewer, B. J., Treu, T., Pancoast, A., Barth, A. J., Bennert, V. N., Bentz, M. C., et al. (2011). The Mass of the Black Hole in Arp 151 from Bayesian Modeling of Reverberation Mapping Data. *ApJ* 733, L33. doi:10.1088/2041-8205/733/2/L33
- Buisson, D. J. K., Parker, M. L., Kara, E., Vasudevan, R. V., Lohfink, A. M., Pinto, C., et al. (2018). NuSTAR observations of Mrk 766: distinguishing reflection from absorption. *MNRAS* 480, 3689–3701. doi:10.1093/mnras/sty2081
- Bustamante, S. and Springel, V. (2019). Spin evolution and feedback of supermassive black holes in cosmological simulations. *MNRAS* 490, 4133–4153. doi:10.1093/mnras/stz2836
- Bîrzan, L., Rafferty, D. A., McNamara, B. R., Wise, M. W., and Nulsen, P. E. J. (2004). A systematic study of radio-induced x-ray cavities in clusters, groups, and galaxies. *The Astrophysical Journal* 607, 800. doi:10.1086/383519
- Cackett, E. M., Chiang, C.-Y., McHardy, I., Edelson, R., Goad, M. R., Horne, K., et al. (2018). Accretion Disk Reverberation with Hubble Space Telescope Observations of NGC 4593: Evidence for Diffuse Continuum Lags. *ApJ* 857, 53. doi:10.3847/1538-4357/aab4f7
- Carter, B. (1971). Axisymmetric Black Hole Has Only Two Degrees of Freedom. *Physical Review Letters* 26, 331–333. doi:10.1103/PhysRevLett.26.331
- Chamani, W., Koljonen, K., and Savolainen, T. (2020). Joint XMM-Newton and NuSTAR observations of the reflection spectrum of III Zw 2. *A&A* 635, A172. doi:10.1051/0004-6361/201936992
- Choudhury, K., García, J. A., Steiner, J. F., and Bambi, C. (2017). Testing the Performance and Accuracy of the RELXILL Model for the Relativistic X-Ray Reflection from Accretion Disks. *ApJ* 851, 57. doi:10.3847/1538-4357/aa9925
- Cicone, C., Maiolino, R., Sturm, E., Graciá-Carpio, J., Feruglio, C., Neri, R., et al. (2014). Massive molecular outflows and evidence for AGN feedback from CO observations. *A&A* 562, A21. doi:10.1051/0004-6361/201322464
- Cole, S., Lacey, C. G., Baugh, C. M., and Frenk, C. S. (2000). Hierarchical galaxy formation. *MNRAS* 319, 168–204. doi:10.1046/j.1365-8711.2000.03879.x
- Crain, R. A. and van de Voort, F. (2023). Hydrodynamical Simulations of the Galaxy Population: Enduring Successes and Outstanding Challenges. *ARA&A* 61, 473–515. doi:10.1146/annurev-astro-041923-043618
- Croton, D. J., Springel, V., White, S. D. M., De Lucia, G., Frenk, C. S., Gao, L., et al. (2006). The many lives of active galactic nuclei: cooling flows, black holes and the luminosities and colours of galaxies. *MNRAS* 365, 11–28. doi:10.1111/j.1365-2966.2005.09675.x
- Curd, B. and Narayan, R. (2023). GRRMHD simulations of MAD accretion discs declining from super-Eddington to sub-Eddington accretion rates. *MNRAS* 518, 3441–3461. doi:10.1093/mnras/stac3330
- Dauser, T., García, J., Parker, M. L., Fabian, A. C., and Wilms, J. (2014). The role of the reflection fraction in constraining black hole spin. *MNRAS* 444, L100–L104. doi:10.1093/mnras/flu125
- Dauser, T., García, J., and Wilms, J. (2016). Relativistic reflection: Review and recent developments in modeling. *Astronomische Nachrichten* 337, 362. doi:10.1002/asna.201612314
- Dauser, T., Wilms, J., Reynolds, C. S., and Brenneman, L. W. (2010). Broad emission lines for a negatively spinning black hole. *MNRAS* 409, 1534–1540. doi:10.1111/j.1365-2966.2010.17393.x
- de La Calle Pérez, I., Longinotti, A. L., Guainazzi, M., Bianchi, S., Dovčiak, M., Cappi, M., et al. (2010). FEROS: Finding extreme relativistic objects. I. Statistics of relativistic Fe K $_{\alpha}$ lines in radio-quiet Type 1 AGN. *A&A* 524, A50. doi:10.1051/0004-6361/200913798

- De Marco, B., Ponti, G., Cappi, M., Dadina, M., Uttley, P., Cackett, E. M., et al. (2013). Discovery of a relation between black hole mass and soft X-ray time lags in active galactic nuclei. *MNRAS* 431, 2441–2452. doi:10.1093/mnras/stt339
- Debattista, V. P., Mayer, L., Carollo, C. M., Moore, B., Wadsley, J., and Quinn, T. (2006). The Secular Evolution of Disk Structural Parameters. *ApJ* 645, 209–227. doi:10.1086/504147
- Di Matteo, T., Springel, V., and Hernquist, L. (2005). Energy input from quasars regulates the growth and activity of black holes and their host galaxies. *Nat* 433, 604–607. doi:10.1038/nature03335
- Dotti, M., Colpi, M., Pallini, S., Perego, A., and Volonteri, M. (2013). On the Orientation and Magnitude of the Black Hole Spin in Galactic Nuclei. *ApJ* 762, 68. doi:10.1088/0004-637X/762/2/68
- Draghis, P. A., Miller, J. M., Zoghbi, A., Reynolds, M., Costantini, E., Gallo, L. C., et al. (2023). A Systematic View of Ten New Black Hole Spins. *ApJ* 946, 19. doi:10.3847/1538-4357/aca7e7
- Dubois, Y., Beckmann, R., Bournaud, F., Choi, H., Devriendt, J., Jackson, R., et al. (2021). Introducing the NEWHORIZON simulation: Galaxy properties with resolved internal dynamics across cosmic time. *A&A* 651, A109. doi:10.1051/0004-6361/202039429
- Dubois, Y., Peirani, S., Pichon, C., Devriendt, J., Gavazzi, R., Welker, C., et al. (2016). The HORIZON-AGN simulation: morphological diversity of galaxies promoted by AGN feedback. *MNRAS* 463, 3948–3964. doi:10.1093/mnras/stw2265
- Dubois, Y., Pichon, C., Welker, C., Le Borgne, D., Devriendt, J., Laigle, C., et al. (2014a). Dancing in the dark: galactic properties trace spin swings along the cosmic web. *MNRAS* 444, 1453–1468. doi:10.1093/mnras/stu1227
- Dubois, Y., Volonteri, M., and Silk, J. (2014b). Black hole evolution - III. Statistical properties of mass growth and spin evolution using large-scale hydrodynamical cosmological simulations. *MNRAS* 440, 1590–1606. doi:10.1093/mnras/stu373
- Dubois, Y., Volonteri, M., Silk, J., Devriendt, J., and Slyz, A. (2014c). Black hole evolution - II. Spinning black holes in a supernova-driven turbulent interstellar medium. *MNRAS* 440, 2333–2346. doi:10.1093/mnras/stu425
- Duro, R., Dauser, T., Wilms, J., Pottschmidt, K., Nowak, M. A., Fritz, S., et al. (2011). The broad iron $K\alpha$ line of Cygnus X-1 as seen by XMM-Newton in the EPIC-pn modified timing mode. *A&A* 533, L3. doi:10.1051/0004-6361/201117446
- Edelson, R., Gelbord, J., Cackett, E., Peterson, B. M., Horne, K., Barth, A. J., et al. (2019). The First Swift Intensive AGN Accretion Disk Reverberation Mapping Survey. *ApJ* 870, 123. doi:10.3847/1538-4357/aaf3b4
- Eraerds, T., Antonelli, V., Davis, C., Hall, D., Hetherington, O., Holland, A., et al. (2021). Enhanced simulations on the Athena/Wide Field Imager instrumental background. *Journal of Astronomical Telescopes, Instruments, and Systems* 7, 034001. doi:10.1117/1.JATIS.7.3.034001
- Esin, A. A., McClintock, J. E., and Narayan, R. (1997). Advection-Dominated Accretion and the Spectral States of Black Hole X-Ray Binaries: Application to Nova Muscae 1991. *ApJ* 489, 865–889. doi:10.1086/304829
- Event Horizon Telescope Collaboration, Akiyama, K., Alberdi, A., Alef, W., Algaba, J. C., Anantua, R., et al. (2022). First Sagittarius A* Event Horizon Telescope Results. I. The Shadow of the Supermassive Black Hole in the Center of the Milky Way. *ApJ* 930, L12. doi:10.3847/2041-8213/ac6674
- Event Horizon Telescope Collaboration, Akiyama, K., Alberdi, A., Alef, W., Asada, K., Azulay, R., et al. (2019). First M87 Event Horizon Telescope Results. I. The Shadow of the Supermassive Black Hole. *ApJ* 875, L1. doi:10.3847/2041-8213/ab0ec7

- Fabian, A. C. (2012). Observational Evidence of Active Galactic Nuclei Feedback. *ARA&A* 50, 455–489. doi:10.1146/annurev-astro-081811-125521
- Fabian, A. C., Iwasawa, K., Reynolds, C. S., and Young, A. J. (2000). Broad Iron Lines in Active Galactic Nuclei. *PASP* 112, 1145–1161. doi:10.1086/316610
- Fabian, A. C., Lohfink, A., Kara, E., Parker, M. L., Vasudevan, R., and Reynolds, C. S. (2015). Properties of AGN coronae in the NuSTAR era. *MNRAS* 451, 4375–4383. doi:10.1093/mnras/stv1218
- Fabian, A. C., Rees, M. J., Stella, L., and White, N. E. (1989). X-ray fluorescence from the inner disc in Cygnus X-1. *MNRAS* 238, 729–736
- Fabian, A. C., Zoghbi, A., Ross, R. R., Uttley, P., Gallo, L. C., Brandt, W. N., et al. (2009). Broad line emission from iron K- and L-shell transitions in the active galaxy 1H0707-495. *Nat* 459, 540–542. doi:10.1038/nature08007
- Faucher-Giguère, C.-A. and Quataert, E. (2012). The physics of galactic winds driven by active galactic nuclei. *MNRAS* 425, 605–622. doi:10.1111/j.1365-2966.2012.21512.x
- Fausnaugh, M. M., Denney, K. D., Barth, A. J., Bentz, M. C., Bottorff, M. C., Carini, M. T., et al. (2016). Space Telescope and Optical Reverberation Mapping Project. III. Optical Continuum Emission and Broadband Time Delays in NGC 5548. *ApJ* 821, 56. doi:10.3847/0004-637X/821/1/56
- Ferrarese, L. and Merritt, D. (2000). A Fundamental Relation between Supermassive Black Holes and Their Host Galaxies. *ApJL* 539, L9–L12. doi:10.1086/312838
- Feruglio, C., Maiolino, R., Piconcelli, E., Menci, N., Aussel, H., Lamastra, A., et al. (2010). Quasar feedback revealed by giant molecular outflows. *A&A* 518, L155. doi:10.1051/0004-6361/201015164
- Fiacconi, D., Sijacki, D., and Pringle, J. E. (2018). Galactic nuclei evolution with spinning black holes: method and implementation. *MNRAS* 477, 3807–3835. doi:10.1093/mnras/sty893
- Fiore, F., Feruglio, C., Shankar, F., Bischetti, M., Bongiorno, A., Brusa, M., et al. (2017). AGN wind scaling relations and the co-evolution of black holes and galaxies. *A&A* 601, A143. doi:10.1051/0004-6361/201629478
- Gallo, L. C., Miniutti, G., Miller, J. M., Brenneman, L. W., Fabian, A. C., Guainazzi, M., et al. (2011). Multi-epoch X-ray observations of the Seyfert 1.2 galaxy Mrk 79: bulk motion of the illuminating X-ray source. *MNRAS* 411, 607–619. doi:10.1111/j.1365-2966.2010.17705.x
- García, J., Dauser, T., Lohfink, A., Kallman, T. R., Steiner, J. F., McClintock, J. E., et al. (2014). Improved Reflection Models of Black Hole Accretion Disks: Treating the Angular Distribution of X-Rays. *ApJ* 782, 76. doi:10.1088/0004-637X/782/2/76
- García, J. and Kallman, T. R. (2010). X-ray Reflected Spectra from Accretion Disk Models. I. Constant Density Atmospheres. *ApJ* 718, 695–706. doi:10.1088/0004-637X/718/2/695
- García, J. A., Kara, E., Walton, D., Beuchert, T., Dauser, T., Gattuzz, E., et al. (2019). Implications of the Warm Corona and Relativistic Reflection Models for the Soft Excess in Mrk 509. *ApJ* 871, 88. doi:10.3847/1538-4357/aaf739
- García, J. A., Steiner, J. F., McClintock, J. E., Remillard, R. A., Grinberg, V., and Dauser, T. (2015). X-Ray Reflection Spectroscopy of the Black Hole GX 339–4: Exploring the Hard State with Unprecedented Sensitivity. *ApJ* 813, 84. doi:10.1088/0004-637X/813/2/84
- García-Burillo, S., Combes, F., Schinnerer, E., Boone, F., and Hunt, L. K. (2005). Molecular gas in Nuclei of GALaxies (NUGA). IV. Gravitational torques and AGN feeding. *A&A* 441, 1011–1030. doi:10.1051/0004-6361:20052900
- Gardner, J. P., Mather, J. C., Abbott, R., Abell, J. S., Abernathy, M., Abney, F. E., et al. (2023). The James Webb Space Telescope Mission. *PASP* 135, 068001. doi:10.1088/1538-3873/acd1b5

- Gebhardt, K., Richstone, D., Kormendy, J., Lauer, T. R., Ajhar, E. A., Bender, R., et al. (2000). Axisymmetric, Three-Integral Models of Galaxies: A Massive Black Hole in NGC 3379. *AJ* 119, 1157–1171. doi:10.1086/301240
- Gehrels, N., Chincarini, G., Giommi, P., Mason, K. O., Nousek, J. A., Wells, A. A., et al. (2004). The Swift Gamma-Ray Burst Mission. *ApJ* 611, 1005–1020. doi:10.1086/422091
- Genzel, R., Eisenhauer, F., and Gillessen, S. (2010). The Galactic Center massive black hole and nuclear star cluster. *Reviews of Modern Physics* 82, 3121–3195. doi:10.1103/RevModPhys.82.3121
- George, I. M. and Fabian, A. C. (1991). X-ray reflection from cold matter in active galactic nuclei and X-ray binaries. *MNRAS* 249, 352–367
- Ghez, A. M., Klein, B. L., Morris, M., and Becklin, E. E. (1998). High Proper-Motion Stars in the Vicinity of Sagittarius A*: Evidence for a Supermassive Black Hole at the Center of Our Galaxy. *ApJ* 509, 678–686. doi:10.1086/306528
- Ghez, A. M., Salim, S., Weinberg, N. N., Lu, J. R., Do, T., Dunn, J. K., et al. (2008). Measuring Distance and Properties of the Milky Way's Central Supermassive Black Hole with Stellar Orbits. *ApJ* 689, 1044–1062. doi:10.1086/592738
- Giustini, M. and Proga, D. (2019). A global view of the inner accretion and ejection flow around super massive black holes. Radiation-driven accretion disk winds in a physical context. *A&A* 630, A94. doi:10.1051/0004-6361/201833810
- Gravity Collaboration, Abuter, R., Amorim, A., Anugu, N., Bauböck, M., Benisty, M., et al. (2018). Detection of the gravitational redshift in the orbit of the star S2 near the Galactic centre massive black hole. *A&A* 615, L15. doi:10.1051/0004-6361/201833718
- GRAVITY Collaboration, Amorim, A., Bauböck, M., Brandner, W., Bolzer, M., Clénet, Y., et al. (2021). The central parsec of NGC 3783: a rotating broad emission line region, asymmetric hot dust structure, and compact coronal line region. *A&A* 648, A117. doi:10.1051/0004-6361/202040061
- GRAVITY Collaboration, Amorim, A., Brandner, W., Clénet, Y., Davies, R., de Zeeuw, P. T., et al. (2020). The spatially resolved broad line region of IRAS 09149-6206. *arXiv e-prints*, arXiv:2009.08463
- Guo, W.-J., Li, Y.-R., Zhang, Z.-X., Ho, L. C., and Wang, J.-M. (2022). Accretion Disk Size Measurements of Active Galactic Nuclei Monitored by the Zwicky Transient Facility. *ApJ* 929, 19. doi:10.3847/1538-4357/ac4e84
- Harikane, Y., Zhang, Y., Nakajima, K., Ouchi, M., Isobe, Y., Ono, Y., et al. (2023). JWST/NIRSpec First Census of Broad-Line AGNs at $z=4-7$: Detection of 10 Faint AGNs with $M_{\text{BH}}=10^6-10^7 M_{\text{sun}}$ and Their Host Galaxy Properties. *arXiv e-prints*, arXiv:2303.11946doi:10.48550/arXiv.2303.11946
- Healy, J., Lousto, C. O., and Zlochower, Y. (2014). Remnant mass, spin, and recoil from spin aligned black-hole binaries. *Phys. Rev. D* 90, 104004. doi:10.1103/PhysRevD.90.104004
- Henriques, B. M. B., White, S. D. M., Lilly, S. J., Bell, E. F., Bluck, A. F. L., and Terrazas, B. A. (2019). The origin of the mass scales for maximal star formation efficiency and quenching: the critical role of supernovae. *MNRAS* 485, 3446–3456. doi:10.1093/mnras/stz577
- Hlavacek-Larrondo, J., Fabian, A. C., Edge, A. C., Ebeling, H., Sanders, J. S., Hogan, M. T., et al. (2012). Extreme AGN feedback in the MAssive Cluster Survey: a detailed study of X-ray cavities at $z\sim 0.3$. *Monthly Notices of the Royal Astronomical Society* 421, 1360–1384. doi:10.1111/j.1365-2966.2011.20405.x
- Hlavacek-Larrondo, J., McDonald, M., Benson, B. A., Forman, W. R., Allen, S. W., Bleem, L. E., et al. (2015). X-ray cavities in a sample of 83 spt-selected clusters of galaxies: Tracing the evolution of agn feedback in clusters of galaxies out to $z = 1.2$. *The Astrophysical Journal* 805, 35. doi:10.1088/0004-637X/805/1/35

- Hofmann, F., Barausse, E., and Rezzolla, L. (2016). The Final Spin from Binary Black Holes in Quasi-circular Orbits. *ApJ* 825, L19. doi:10.3847/2041-8205/825/2/L19
- Homayouni, Y., Sturm, M. R., Trump, J. R., Horne, K., Grier, C. J., Shen, Y., et al. (2022). The Sloan Digital Sky Survey Reverberation Mapping Project: UV-Optical Accretion Disk Measurements with the Hubble Space Telescope. *ApJ* 926, 225. doi:10.3847/1538-4357/ac478b
- Hopkins, P. F., Hernquist, L., Cox, T. J., Di Matteo, T., Robertson, B., and Springel, V. (2006). A Unified, Merger-Driven Model for the Origin of Starbursts, Quasars, the Cosmic X-Ray Background, Supermassive Black Holes and Galaxy Spheroids. *ASTROPHYS J SUPPL S* 163, 1–49. doi:10.1086/499298. ArXiv:astro-ph/0506398
- Hopkins, P. F., Kereš, D., Oñorbe, J., Faucher-Giguère, C.-A., Quataert, E., Murray, N., et al. (2014). Galaxies on FIRE (Feedback In Realistic Environments): stellar feedback explains cosmologically inefficient star formation. *MNRAS* 445, 581–603. doi:10.1093/mnras/stu1738
- Hopkins, P. F. and Quataert, E. (2010). How do massive black holes get their gas? *MNRAS* 407, 1529–1564. doi:10.1111/j.1365-2966.2010.17064.x
- Hopkins, P. F., Quataert, E., and Murray, N. (2011). Self-regulated star formation in galaxies via momentum input from massive stars. *MNRAS* 417, 950–973. doi:10.1111/j.1365-2966.2011.19306.x
- Hoyle, F. and Lyttleton, R. A. (1939). The effect of interstellar matter on climatic variation. *Proceedings of the Cambridge Philosophical Society* 35, 405. doi:10.1017/S0305004100021150
- Ingram, A., Mastroserio, G., van der Klis, M., Nathan, E., Connors, R., Dauser, T., et al. (2022). On measuring the Hubble constant with X-ray reverberation mapping of active galactic nuclei. *MNRAS* 509, 619–633. doi:10.1093/mnras/stab2950
- Israel, W. (1967). Event Horizons in Static Vacuum Space-Times. *Physical Review* 164, 1776–1779. doi:10.1103/PhysRev.164.1776
- Israel, W. (1968). Event horizons in static electrovac space-times. *Communications in Mathematical Physics* 8, 245–260. doi:10.1007/BF01645859
- Jiang, J., Buisson, D. J. K., Dauser, T., Fabian, A. C., Fürst, F., Gallo, L. C., et al. (2022). A NuSTAR and Swift view of the hard state of MAXI J1813-095. *MNRAS* 514, 1952–1960. doi:10.1093/mnras/stac1401
- Jiang, J., Fabian, A. C., Dauser, T., Gallo, L., García, J. A., Kara, E., et al. (2019). High Density Reflection Spectroscopy - II. The density of the inner black hole accretion disc in AGN. *MNRAS* 489, 3436–3455. doi:10.1093/mnras/stz2326
- Jiang, J., Parker, M. L., Fabian, A. C., Alston, W. N., Buisson, D. J. K., Cackett, E. M., et al. (2018). The 1.5 Ms observing campaign on IRAS 13224-3809 - I. X-ray spectral analysis. *MNRAS* 477, 3711–3726. doi:10.1093/mnras/sty836
- Jiang, Y.-F., Green, P. J., Greene, J. E., Morganson, E., Shen, Y., Pancoast, A., et al. (2017). Detection of Time Lags between Quasar Continuum Emission Bands Based On Pan-STARRS Light Curves. *ApJ* 836, 186. doi:10.3847/1538-4357/aa5b91
- Kammoun, E. S., Nardini, E., and Risaliti, G. (2018). Testing the accuracy of reflection-based supermassive black hole spin measurements in AGN. *A&A* 614, A44. doi:10.1051/0004-6361/201732377
- Kara, E., Alston, W. N., Fabian, A. C., Cackett, E. M., Uttley, P., Reynolds, C. S., et al. (2016). A global look at X-ray time lags in Seyfert galaxies. *MNRAS* 462, 511–531. doi:10.1093/mnras/stw1695
- Kara, E., Steiner, J. F., Fabian, A. C., Cackett, E. M., Uttley, P., Remillard, R. A., et al. (2019). The corona contracts in a black-hole transient. *Nat* 565, 198–201. doi:10.1038/s41586-018-0803-x
- Katz, N., Weinberg, D. H., and Hernquist, L. (1996). Cosmological Simulations with TreeSPH. *ApJS* 105, 19. doi:10.1086/192305

- Kaviraj, S., Laigle, C., Kimm, T., Devriendt, J. E. G., Dubois, Y., Pichon, C., et al. (2017). The Horizon-AGN simulation: evolution of galaxy properties over cosmic time. *MNRAS* 467, 4739–4752. doi:10.1093/mnras/stx126
- Kereš, D., Katz, N., Weinberg, D. H., and Davé, R. (2005). How do galaxies get their gas? *MNRAS* 363, 2–28. doi:10.1111/j.1365-2966.2005.09451.x
- Kesden, M. (2008). Can binary mergers produce maximally spinning black holes? *Phys. Rev. D* 78, 084030. doi:10.1103/PhysRevD.78.084030
- King, A. L., Walton, D. J., Miller, J. M., Barret, D., Boggs, S. E., Christensen, F. E., et al. (2014). The Disk Wind in the Rapidly Spinning Stellar-mass Black Hole 4U 1630-472 Observed with NuSTAR. *ApJ* 784, L2. doi:10.1088/2041-8205/784/1/L2
- King, A. R., Pringle, J. E., and Hofmann, J. A. (2008). The evolution of black hole mass and spin in active galactic nuclei. *MNRAS* 385, 1621–1627. doi:10.1111/j.1365-2966.2008.12943.x
- Kollmeier, J., Anderson, S. F., Blanc, G. A., Blanton, M. R., Covey, K. R., Crane, J., et al. (2019). SDSS-V Pioneering Panoptic Spectroscopy. In *Bulletin of the American Astronomical Society*. vol. 51, 274
- Komatsu, E., Smith, K. M., Dunkley, J., Bennett, C. L., Gold, B., Hinshaw, G., et al. (2011). Seven-year Wilkinson Microwave Anisotropy Probe (WMAP) Observations: Cosmological Interpretation. *ApJS* 192, 18. doi:10.1088/0067-0049/192/2/18
- Kormendy, J., Bender, R., Evans, A. S., and Richstone, D. (1998). The Mass Distribution in the Elliptical Galaxy NGC 3377: Evidence for a $2 \times 10^8 M_{\odot}$ Black Hole. *AJ* 115, 1823–1839. doi:10.1086/300313
- Kormendy, J. and Ho, L. C. (2013). Coevolution (Or Not) of Supermassive Black Holes and Host Galaxies. *ARA&A* 51, 511–653. doi:10.1146/annurev-astro-082708-101811
- Koss, M., Trakhtenbrot, B., Ricci, C., Lamperti, I., Oh, K., Berney, S., et al. (2017). BAT AGN Spectroscopic Survey. I. Spectral Measurements, Derived Quantities, and AGN Demographics. *ApJ* 850, 74. doi:10.3847/1538-4357/aa8ec9
- Koss, M. J., Trakhtenbrot, B., Ricci, C., Oh, K., Bauer, F. E., Stern, D., et al. (2022). VizieR Online Data Catalog: BASS. XXV. DR2 stellar velocity dispersions (Koss+, 2022). *VizieR Online Data Catalog*, J/ApJS/261/6doi:10.26093/cds/vizie.22610006
- Kuijken, K. and Merrifield, M. R. (1995). Establishing the Connection between Peanut-shaped Bulges and Galactic Bars. *ApJ* 443, L13. doi:10.1086/187824
- Laor, A. (1991). Line profiles from a disk around a rotating black hole. *ApJ* 376, 90–94. doi:10.1086/170257
- Liska, M., Tchekhovskoy, A., Ingram, A., and van der Klis, M. (2019). Bardeen-Petterson alignment, jets, and magnetic truncation in GRMHD simulations of tilted thin accretion discs. *MNRAS* 487, 550–561. doi:10.1093/mnras/stz834
- Lowell, B., Jacquemin-Ide, J., Tchekhovskoy, A., and Duncan, A. (2023). Rapid Black Hole Spin-down by Thick Magnetically Arrested Disks. *arXiv e-prints*, arXiv:2302.01351doi:10.48550/arXiv.2302.01351
- Magdziarz, P. and Zdziarski, A. A. (1995). Angle-dependent Compton reflection of X-rays and gamma-rays. *MNRAS* 273, 837–848
- Magorrian, J., Tremaine, S., Richstone, D., Bender, R., Bower, G., Dressler, A., et al. (1998). The Demography of Massive Dark Objects in Galaxy Centers. *AJ* 115, 2285–2305. doi:10.1086/300353
- Maiolino, R., Gallerani, S., Neri, R., Cicone, C., Ferrara, A., Genzel, R., et al. (2012). Evidence of strong quasar feedback in the early Universe. *MNRAS* 425, L66–L70. doi:10.1111/j.1745-3933.2012.01303.x
- Maiolino, R., Scholtz, J., Curtis-Lake, E., Carniani, S., Baker, W., de Graaff, A., et al. (2023a). JADES. The diverse population of infant Black Holes at $4 < z < 11$: merging, tiny, poor, but mighty. *arXiv e-prints*, arXiv:2308.01230doi:10.48550/arXiv.2308.01230

- Maiolino, R., Scholtz, J., Witstok, J., Carniani, S., D'Eugenio, F., de Graaff, A., et al. (2023b). A small and vigorous black hole in the early Universe. *arXiv e-prints*, arXiv:2305.12492doi:10.48550/arXiv.2305.12492
- Mallick, L., Fabian, A. C., García, J. A., Tomsick, J. A., Parker, M. L., Dauser, T., et al. (2022). High-density disc reflection spectroscopy of low-mass active galactic nuclei. *MNRAS* 513, 4361–4379. doi:10.1093/mnras/stac990
- Mallick, L., Wilkins, D. R., Alston, W. N., Markowitz, A., De Marco, B., Parker, M. L., et al. (2021). Discovery of soft and hard X-ray time lags in low-mass AGNs. *MNRAS* 503, 3775–3783. doi:10.1093/mnras/stab627
- Marinucci, A., Matt, G., Kara, E., Miniutti, G., Elvis, M., Arevalo, P., et al. (2014). Simultaneous NuSTAR and XMM-Newton 0.5–80 keV spectroscopy of the narrow-line Seyfert 1 galaxy SWIFT J2127.4+5654. *MNRAS* 440, 2347–2356. doi:10.1093/mnras/stu404
- Massonneau, W., Volonteri, M., Dubois, Y., and Beckmann, R. S. (2023). How the super-Eddington regime regulates black hole growth in high-redshift galaxies. *A&A* 670, A180. doi:10.1051/0004-6361/202243170
- McConnell, N. J. and Ma, C.-P. (2013). Revisiting the Scaling Relations of Black Hole Masses and Host Galaxy Properties. *ApJ* 764, 184. doi:10.1088/0004-637X/764/2/184
- McKinney, J. C., Tchekhovskoy, A., and Blandford, R. D. (2012). General relativistic magnetohydrodynamic simulations of magnetically choked accretion flows around black holes. *Monthly Notices of the Royal Astronomical Society* 423, 3083–3117. doi:10.1111/j.1365-2966.2012.21074.x
- McNamara, B. R., Wise, M., Nulsen, P. E. J., David, L. P., Sarazin, C. L., Bautz, M., et al. (2000). Chandra X-Ray Observations of the Hydra A Cluster: An Interaction between the Radio Source and the X-Ray-emitting Gas. *ApJ* 534, L135–L138. doi:10.1086/312662
- Meidinger, N., Albrecht, S., Beitler, C., Bonholzer, M., Emberger, V., Frank, J., et al. (2020). Development status of the wide field imager instrument for Athena. In *Space Telescopes and Instrumentation 2020: Ultraviolet to Gamma Ray*, eds. J.-W. A. den Herder, S. Nikzad, and K. Nakazawa. vol. 11444 of *Society of Photo-Optical Instrumentation Engineers (SPIE) Conference Series*, 114440T. doi:10.1117/12.2560507
- Merloni, A. and Fabian, A. C. (2001). Accretion disc coronae as magnetic reservoirs. *MNRAS* 321, 549–552. doi:10.1046/j.1365-8711.2001.04060.x
- Michel, F. C. (1972). Accretion of Matter by Condensed Objects. *Astrophysics and Space Science* 15, 153–160. doi:10.1007/BF00649949
- Miller, J. M., Reynolds, C. S., Fabian, A. C., Miniutti, G., and Gallo, L. C. (2009). Stellar-Mass Black Hole Spin Constraints from Disk Reflection and Continuum Modeling. *ApJ* 697, 900–912. doi:10.1088/0004-637X/697/1/900
- Miniutti, G., Fabian, A. C., and Miller, J. M. (2004). The relativistic Fe emission line in XTE J1650-500 with BeppoSAX: evidence for black hole spin and light-bending effects? *MNRAS* 351, 466–472. doi:10.1111/j.1365-2966.2004.07794.x
- Miniutti, G., Ponti, G., Dadina, M., Cappi, M., and Malaguti, G. (2007). IRAS 13197-1627 has them all: Compton-thin absorption, photoionized gas, thermal plasmas and a broad Fe line. *MNRAS* 375, 227–239. doi:10.1111/j.1365-2966.2006.11291.x
- Moderski, R. and Sikora, M. (1996). On black hole evolution in active galactic nuclei. *MNRAS* 283, 854–864. doi:10.1093/mnras/283.3.854
- Moderski, R., Sikora, M., and Lasota, J. P. (1998). On the spin paradigm and the radio dichotomy of quasars. *MNRAS* 301, 142–148. doi:10.1046/j.1365-8711.1998.02009.x

- Murray, N., Chiang, J., Grossman, S. A., and Voit, G. M. (1995). Accretion Disk Winds from Active Galactic Nuclei. *ApJ* 451, 498. doi:10.1086/176238
- Nandra, K., Barret, D., Barcons, X., Fabian, A., den Herder, J.-W., Piro, L., et al. (2013). The Hot and Energetic Universe: A White Paper presenting the science theme motivating the Athena+ mission. *arXiv e-prints*, arXiv:1306.2307doi:10.48550/arXiv.1306.2307
- Narayan, R., Chael, A., Chatterjee, K., Ricarte, A., and Curd, B. (2022). Jets in magnetically arrested hot accretion flows: geometry, power, and black hole spin-down. *Monthly Notices of the Royal Astronomical Society* 511, 3795–3813. doi:10.1093/mnras/stac285
- Narayan, R. and Yi, I. (1994). Advection-dominated Accretion: A Self-similar Solution. *ApJ* 428, L13. doi:10.1086/187381
- Nardini, E., Fabian, A. C., Reis, R. C., and Walton, D. J. (2011). A reflection origin for the soft and hard X-ray excess of Ark 120. *MNRAS* 410, 1251–1261. doi:10.1111/j.1365-2966.2010.17518.x
- Novikov, I. D. and Frolov, V. P. (1989). *Physics of black holes*
- Novikov, I. D. and Thorne, K. S. (1973). Astrophysics of black holes. In *Black Holes (Les Astres Occlus)*. 343–450
- Oh, K., Koss, M., Markwardt, C. B., Schawinski, K., Baumgartner, W. H., Barthelmy, S. D., et al. (2018). The 105-Month Swift-BAT All-sky Hard X-Ray Survey. *ApJS* 235, 4. doi:10.3847/1538-4365/aaa7fd
- Pancoast, A., Brewer, B. J., and Treu, T. (2014). Modelling reverberation mapping data - I. Improved geometric and dynamical models and comparison with cross-correlation results. *MNRAS* 445, 3055–3072. doi:10.1093/mnras/stu1809
- Parker, M. L., Wilkins, D. R., Fabian, A. C., Grupe, D., Dauser, T., Matt, G., et al. (2014). The NuSTAR spectrum of Mrk 335: extreme relativistic effects within two gravitational radii of the event horizon? *MNRAS* 443, 1723–1732. doi:10.1093/mnras/stu1246
- Penna, R. F., McKinney, J. C., Narayan, R., Tchekhovskoy, A., Shafee, R., and McClintock, J. E. (2010). Simulations of magnetized discs around black holes: effects of black hole spin, disc thickness and magnetic field geometry. *MNRAS* 408, 752–782. doi:10.1111/j.1365-2966.2010.17170.x
- Peterson, B. M. (1993). Reverberation Mapping of Active Galactic Nuclei. *PASP* 105, 247. doi:10.1086/133140
- Peterson, B. M., Ferrarese, L., Gilbert, K. M., Kaspi, S., Malkan, M. A., Maoz, D., et al. (2004). Central Masses and Broad-Line Region Sizes of Active Galactic Nuclei. II. A Homogeneous Analysis of a Large Reverberation-Mapping Database. *ApJ* 613, 682–699. doi:10.1086/423269
- Piotrowska, J. M., Bluck, A. F. L., Maiolino, R., and Peng, Y. (2022). On the quenching of star formation in observed and simulated central galaxies: evidence for the role of integrated AGN feedback. *MNRAS* 512, 1052–1090. doi:10.1093/mnras/stab3673
- Ponti, G., Papadakis, I., Bianchi, S., Guainazzi, M., Matt, G., Uttley, P., et al. (2012). CAIXA: a catalogue of AGN in the XMM-Newton archive. III. Excess variance analysis. *A&A* 542, A83. doi:10.1051/0004-6361/201118326
- Putman, M. E., Peek, J. E. G., and Joung, M. R. (2012). Gaseous Galaxy Halos. *ARA&A* 50, 491–529. doi:10.1146/annurev-astro-081811-125612
- Reis, R. C., Fabian, A. C., Ross, R. R., and Miller, J. M. (2009). Determining the spin of two stellar-mass black holes from disc reflection signatures. *MNRAS* 395, 1257–1264. doi:10.1111/j.1365-2966.2009.14622.x
- Reis, R. C. and Miller, J. M. (2013). On the Size and Location of the X-Ray Emitting Coronae around Black Holes. *ApJ* 769, L7. doi:10.1088/2041-8205/769/1/L7

- Reis, R. C., Reynolds, M. T., Miller, J. M., and Walton, D. J. (2014). Reflection from the strong gravity regime in a lensed quasar at redshift $z = 0.658$. *Nat* 507, 207–209. doi:10.1038/nature13031
- Reynolds, C. S. (2021). Observational Constraints on Black Hole Spin. *ARA&A* 59, 117–154. doi:10.1146/annurev-astro-112420-035022
- Reynolds, C. S., Brenneman, L. W., Lohfink, A. M., Trippe, M. L., Miller, J. M., Reis, R. C., et al. (2012). Probing relativistic astrophysics around SMBHs: The Suzaku AGN spin survey. In *Suzaku 2011: Exploring the X-ray Universe: Suzaku and Beyond*, eds. R. Petre, K. Mitsuda, and L. Angelini. vol. 1427 of *American Institute of Physics Conference Series*, 157–164. doi:10.1063/1.3696170
- Reynolds, M. T., Walton, D. J., Miller, J. M., and Reis, R. C. (2014). A Rapidly Spinning Black Hole Powers the Einstein Cross. *ApJ* 792, L19. doi:10.1088/2041-8205/792/1/L19
- Rezzolla, L., Diener, P., Dorband, E. N., Pollney, D., Reisswig, C., Schnetter, E., et al. (2008). The Final Spin from the Coalescence of Aligned-Spin Black Hole Binaries. *ApJ* 674, L29. doi:10.1086/528935
- Ricci, C., Tazaki, F., Ueda, Y., Paltani, S., Boissay, R., and Terashima, Y. (2014). Suzaku Observation of IRAS 00521-7054, a Peculiar Type-II AGN with a Very Broad Feature at 6 keV. *ApJ* 795, 147. doi:10.1088/0004-637X/795/2/147
- Ricci, C., Trakhtenbrot, B., Koss, M. J., Ueda, Y., Del Vecchio, I., Treister, E., et al. (2017). BAT AGN Spectroscopic Survey. V. X-Ray Properties of the Swift/BAT 70-month AGN Catalog. *ApJS* 233, 17. doi:10.3847/1538-4365/aa96ad
- Rigby, J., Perrin, M., McElwain, M., Kimble, R., Friedman, S., Lallo, M., et al. (2023). The Science Performance of JWST as Characterized in Commissioning. *PASP* 135, 048001. doi:10.1088/1538-3873/acb293
- Risaliti, G., Harrison, F. A., Madsen, K. K., Walton, D. J., Boggs, S. E., Christensen, F. E., et al. (2013). A rapidly spinning supermassive black hole at the centre of NGC1365. *Nat* 494, 449–451. doi:10.1038/nature11938
- Ross, R. R. and Fabian, A. C. (2005). A comprehensive range of X-ray ionized-reflection models. *MNRAS* 358, 211–216. doi:10.1111/j.1365-2966.2005.08797.x
- Russell, H. R., Fabian, A. C., McNamara, B. R., and Broderick, A. E. (2015). Inside the Bondi radius of M87. *MNRAS* 451, 588–600. doi:10.1093/mnras/stv954
- Russell, H. R., Fabian, A. C., McNamara, B. R., Miller, J. M., Nulsen, P. E. J., Piotrowska, J. M., et al. (2018). The imprints of AGN feedback within a supermassive black hole’s sphere of influence. *MNRAS* 477, 3583–3599. doi:10.1093/mnras/sty835
- Saglia, R. P., Opitsch, M., Erwin, P., Thomas, J., Beifiori, A., Fabricius, M., et al. (2016). The SINFONI Black Hole Survey: The Black Hole Fundamental Plane Revisited and the Paths of (Co)evolution of Supermassive Black Holes and Bulges. *ApJ* 818, 47. doi:10.3847/0004-637X/818/1/47
- Sancisi, R., Fraternali, F., Oosterloo, T., and van der Hulst, T. (2008). Cold gas accretion in galaxies. *The Astronomy and Astrophysics Review* 15, 189–223. doi:10.1007/s00159-008-0010-0
- Sanders, D. B., Soifer, B. T., Elias, J. H., Madore, B. F., Matthews, K., Neugebauer, G., et al. (1988). Ultraluminous Infrared Galaxies and the Origin of Quasars. *ApJ* 325, 74. doi:10.1086/165983
- Schwarz, M. P. (1981). The response of gas in a galactic disk to bar forcing. *ApJ* 247, 77–88. doi:10.1086/159011
- Sesana, A., Barausse, E., Dotti, M., and Rossi, E. M. (2014). Linking the Spin Evolution of Massive Black Holes to Galaxy Kinematics. *ApJ* 794, 104. doi:10.1088/0004-637X/794/2/104
- Shakura, N. I. and Sunyaev, R. A. (1973). Black holes in binary systems. Observational appearance. *A&A* 24, 337–355

- Sisk-Reynés, J., Reynolds, C. S., Matthews, J. H., and Smith, R. N. (2022). Evidence for a moderate spin from X-ray reflection of the high-mass supermassive black hole in the cluster-hosted quasar H1821+643. *MNRAS* 514, 2568–2580. doi:10.1093/mnras/stac1389
- Springel, V. (2010). E pur si muove: Galilean-invariant cosmological hydrodynamical simulations on a moving mesh. *MNRAS* 401, 791–851. doi:10.1111/j.1365-2966.2009.15715.x
- Springel, V., Di Matteo, T., and Hernquist, L. (2005). Black Holes in Galaxy Mergers: The Formation of Red Elliptical Galaxies. *ApJ* 620, L79–L82. doi:10.1086/428772
- Steiner, J. F., McClintock, J. E., Remillard, R. A., Gou, L., Yamada, S., and Narayan, R. (2010). The Constant Inner-disk Radius of LMC X-3: A Basis for Measuring Black Hole Spin. *ApJ* 718, L117–L121. doi:10.1088/2041-8205/718/2/L117
- Talbot, R. Y., Bourne, M. A., and Sijacki, D. (2021). Blandford-Znajek jets in galaxy formation simulations: method and implementation. *MNRAS* 504, 3619–3650. doi:10.1093/mnras/stab804
- Talbot, R. Y., Sijacki, D., and Bourne, M. A. (2022). Blandford-Znajek jets in galaxy formation simulations: exploring the diversity of outflows produced by spin-driven AGN jets in Seyfert galaxies. *MNRAS* 514, 4535–4559. doi:10.1093/mnras/stac1566
- Tanaka, Y., Nandra, K., Fabian, A. C., Inoue, H., Otani, C., Dotani, T., et al. (1995). Gravitationally redshifted emission implying an accretion disk and massive black hole in the active galaxy MCG-6-30-15. *Nat* 375, 659–661. doi:10.1038/375659a0
- Tao, L., Tomsick, J. A., Qu, J., Zhang, S., Zhang, S., and Bu, Q. (2019). The Spin of the Black Hole GRS 1716-249 Determined from the Hard Intermediate State. *ApJ* 887, 184. doi:10.3847/1538-4357/ab5282
- Tchekhovskoy, A., McKinney, J. C., and Narayan, R. (2012). General relativistic modeling of magnetized jets from accreting black holes. *Journal of Physics: Conference Series* 372, 012040. doi:10.1088/1742-6596/372/1/012040
- Tchekhovskoy, A., Narayan, R., and McKinney, J. C. (2011). Efficient generation of jets from magnetically arrested accretion on a rapidly spinning black hole. *MNRAS* 418, L79–L83. doi:10.1111/j.1745-3933.2011.01147.x
- Terrazas, B. A., Bell, E. F., Henriques, B. M. B., White, S. D. M., Cattaneo, A., and Woo, J. (2016). Quiescence Correlates Strongly with Directly Measured Black Hole Mass in Central Galaxies. *ApJL* 830, L12. doi:10.3847/2041-8205/830/1/L12
- Teyssier, R. (2002). Cosmological hydrodynamics with adaptive mesh refinement. A new high resolution code called RAMSES. *A&A* 385, 337–364. doi:10.1051/0004-6361:20011817
- Thorne, K. S. (1974). Disk-Accretion onto a Black Hole. II. Evolution of the Hole. *ApJ* 191, 507–520. doi:10.1086/152991
- Tichy, W. and Marronetti, P. (2008). Final mass and spin of black-hole mergers. *Phys. Rev. D* 78, 081501. doi:10.1103/PhysRevD.78.081501
- Tomsick, J. A., Yamaoka, K., Corbel, S., Kaaret, P., Kalemci, E., and Migliari, S. (2009). Truncation of the Inner Accretion Disk Around a Black Hole at Low Luminosity. *ApJ* 707, L87–L91. doi:10.1088/0004-637X/707/1/L87
- Toomre, A. and Toomre, J. (1972). Galactic Bridges and Tails. *ApJ* 178, 623–666. doi:10.1086/151823
- Treves, A. and Turolla, R. (1999). Vacuum Breakdown near a Black Hole Charged by Hypercritical Accretion. *ApJ* 517, 396–398. doi:10.1086/307159
- Tumlinson, J., Peebles, M. S., and Werk, J. K. (2017). The Circumgalactic Medium. *ARA&A* 55, 389–432. doi:10.1146/annurev-astro-091916-055240
- Villar-Martín, M., Humphrey, A., Delgado, R. G., Colina, L., and Arribas, S. (2011). Ionized outflows in SDSS type 2 quasars at $z \sim 0.3-0.6$. *MNRAS* 418, 2032–2042. doi:10.1111/j.1365-2966.2011.19622.x

- Vogelsberger, M., Marinacci, F., Torrey, P., and Puchwein, E. (2020). Cosmological simulations of galaxy formation. *Nature Reviews Physics* 2, 42–66. doi:10.1038/s42254-019-0127-2
- Volonteri, M., Dubois, Y., Pichon, C., and Devriendt, J. (2016). The cosmic evolution of massive black holes in the Horizon-AGN simulation. *MNRAS* 460, 2979–2996. doi:10.1093/mnras/stw1123
- Wald, R. M. (1984). *General Relativity*
- Walton, D. J., Alston, W. N., Kosec, P., Fabian, A. C., Gallo, L. C., Garcia, J. A., et al. (2020). A full characterization of the supermassive black hole in IRAS 09149-6206. *MNRAS* 499, 1480–1498. doi:10.1093/mnras/staa2961
- Walton, D. J., Baloković, M., Fabian, A. C., Gallo, L. C., Koss, M., Nardini, E., et al. (2021). Extreme relativistic reflection in the active galaxy ESO 033-G002. *MNRAS* 506, 1557–1572. doi:10.1093/mnras/stab1290
- Walton, D. J., Mooley, K., King, A. L., Tomsick, J. A., Miller, J. M., Dauser, T., et al. (2017). Living on a Flare: Relativistic Reflection in V404 Cyg Observed by NuSTAR during Its Summer 2015 Outburst. *ApJ* 839, 110. doi:10.3847/1538-4357/aa67e8
- Walton, D. J., Nardini, E., Fabian, A. C., Gallo, L. C., and Reis, R. C. (2013). Suzaku observations of ‘bare’ active galactic nuclei. *MNRAS* 428, 2901–2920. doi:10.1093/mnras/sts227
- Walton, D. J., Nardini, E., Gallo, L. C., Reynolds, M. T., Ricci, C., Dauser, T., et al. (2019). A low-flux state in IRAS 00521-7054 seen with NuSTAR and XMM-Newton: relativistic reflection and an ultrafast outflow. *MNRAS* 484, 2544–2555. doi:10.1093/mnras/stz115
- Walton, D. J., Reis, R. C., Cackett, E. M., Fabian, A. C., and Miller, J. M. (2012). The similarity of broad iron lines in X-ray binaries and active galactic nuclei. *MNRAS* 422, 2510–2531. doi:10.1111/j.1365-2966.2012.20809.x
- Walton, D. J., Risaliti, G., Harrison, F. A., Fabian, A. C., Miller, J. M., Arevalo, P., et al. (2014). NuSTAR and XMM-Newton Observations of NGC 1365: Extreme Absorption Variability and a Constant Inner Accretion Disk. *ApJ* 788, 76. doi:10.1088/0004-637X/788/1/76
- Weinberger, R., Springel, V., Hernquist, L., Pillepich, A., Marinacci, F., Pakmor, R., et al. (2017). Simulating galaxy formation with black hole driven thermal and kinetic feedback. *MNRAS* 465, 3291–3308. doi:10.1093/mnras/stw2944
- Werner, N., McNamara, B. R., Churazov, E., and Scannapieco, E. (2019). Hot Atmospheres, Cold Gas, AGN Feedback and the Evolution of Early Type Galaxies: A Topical Perspective. *Space Science Reviews* 215, 5. doi:10.1007/s11214-018-0571-9
- Wilkins, D. R., Gallo, L. C., Costantini, E., Brandt, W. N., and Blandford, R. D. (2022). Acceleration and cooling of the corona during X-ray flares from the Seyfert galaxy I Zw 1. *MNRAS* 512, 761–775. doi:10.1093/mnras/stac416
- Wilkins, D. R., Gallo, L. C., Grupe, D., Bonson, K., Komossa, S., and Fabian, A. C. (2015). Flaring from the supermassive black hole in Mrk 335 studied with Swift and NuSTAR. *MNRAS* 454, 4440–4451. doi:10.1093/mnras/stv2130
- Wong, K.-W., Irwin, J. A., Shcherbakov, R. V., Yukita, M., Million, E. T., and Bregman, J. N. (2014). The Megasecond Chandra X-Ray Visionary Project Observation of NGC 3115: Witnessing the Flow of Hot Gas within the Bondi Radius. *ApJ* 780, 9. doi:10.1088/0004-637X/780/1/9
- Wong, K.-W., Irwin, J. A., Yukita, M., Million, E. T., Mathews, W. G., and Bregman, J. N. (2011). Resolving the Bondi Accretion Flow toward the Supermassive Black Hole of NGC 3115 with Chandra. *ApJ* 736, L23. doi:10.1088/2041-8205/736/1/L23
- Woo, J.-H., Yoon, Y., Park, S., Park, D., and Kim, S. C. (2015). The Black Hole Mass-Stellar Velocity Dispersion Relation of Narrow-line Seyfert 1 Galaxies. *ApJ* 801, 38. doi:10.1088/0004-637X/801/1/38

- Xu, Y., Harrison, F. A., García, J. A., Fabian, A. C., Fürst, F., Gandhi, P., et al. (2018). Reflection Spectra of the Black Hole Binary Candidate MAXI J1535-571 in the Hard State Observed by NuSTAR. *ApJ* 852, L34. doi:10.3847/2041-8213/aaa4b2
- Yuan, F. and Narayan, R. (2014). Hot Accretion Flows Around Black Holes. *ARA&A* 52, 529–588. doi:10.1146/annurev-astro-082812-141003
- Zdziarski, A. A., Johnson, W. N., and Magdziarz, P. (1996). Broad-band γ -ray and X-ray spectra of NGC 4151 and their implications for physical processes and geometry. *MNRAS* 283, 193–206
- Zycki, P. T., Done, C., and Smith, D. A. (1999). The 1989 May outburst of the soft X-ray transient GS 2023+338 (V404 Cyg). *MNRAS* 309, 561–575. doi:10.1046/j.1365-8711.1999.02885.x